Chemical Geology 532 (2020) 119378

Contents lists available at ScienceDirect

Chemical Geology

journal homepage: www.elsevier.com/locate/chemgeo

Preference of Co over Al for substitution of Fe in goethite (α-FeOOH) structure: Mechanism revealed from EXAFS, XPS, DFT and linear free energy correlation model

Hui Yin[a], Yanli Wu[a], Jingtao Hou[a], Xinran Yan[a], Zhaohui Li[b], Chuanwei Zhu[c], Jing Zhang[d], Xionghan Feng[a], Wenfeng Tan[a], Fan Liu[a,*]

[a] Key Laboratory of Arable Land Conservation (Middle and Lower Reaches of Yangtse River) Ministry of Agriculture, College of Resources and Environment, Huazhong Agricultural University, Wuhan 430070, China
[b] Geosciences Department, University of Wisconsin – Parkside, Kenosha, WI 53144, USA
[c] State Key Laboratory of Ore Deposit Geochemistry, Institute of Geochemistry, Chinese Academy of Sciences, Guiyang 550002, China
[d] Beijing Synchrotron Radiation Facility, Institute of High Energy Physics, Chinese Academy of Sciences, Beijing 100039, China

ARTICLE INFO

Editor: Hailiang Dong

Keywords:
Iron hydroxides
Goethite
Isomorphous substitution
Cobalt
Linear free energy relationship

ABSTRACT

Goethite is the most stable iron hydroxide mineral in geological environments, and it is usually crystallized with more than one type of substituent. However, the synergetic or antagonistic effects of coexisting cations on substitution for lattice Fe in gothite are unclear. In this study, a series of Co-, Al-, and Co + Al co-substituted goethite samples were synthesized at room temperature and then investigated by powder XRD, X-ray photoelectron spectroscopy (XPS), X-ray absorption fine structure spectroscopy (XAFS), density function theory (DFT) calculations, and acid dissolution experiments. All the obtained samples were pure goethite, except the one with a high total content of Co + Al that contained a portion of 2-line ferrihydrite. Lattice parameter *a* of Co + Al co-substituted goethite was linearly decreased with the final Co content, lattice parameter *b* and calculated crystal density had the best negatively linear relationships with Al content while lattice parameter *c*, cell volume, average edge-sharing Fe − Me (Me = Fe, Al, and Co) distances along c* and b* axis (E′ and E) and average corner-sharing Fe − Me (DC) distances had the best linear correlations with the total contents of Co + Al. Aluminum and Co were found to be evenly distributed in goethite structure, and both reduced the mineral particle size. Co coexisted in a mixed valance of +2 and +3, and the proportion of Co^{3+} increased with the increase of Co content in Co-substituted goethite owing to relatively high electric potential energy and decreased with the increase of coexisting Al^{3+} content in Co + Al co-substituted goethites because of relatively low alkalinity in local environments around Co^{2+}. Incorporation of Co greatly promoted the mineral dissolution in 2 M HCl solution at 298 K. Fe K-edge EXAFS analysis indicated almost constant local order around Fe in these samples. Coexisting Al had almost no effect on Co incorporation into goethite structure but Co suppressed Al substitution for lattice Fe. This preference of Co over Al to substitute for Fe was explained by the predicted partition coefficients (K_d) of common trivalent substituents in goethite by using the linear free energy relationship. It highlights the necessity to take into consideration not only the substituent physical properties (size and charge) but also their chemical properties (chemical bonding energy and chemical potential). These results enhanced our understanding of the incorporation of exotic cations into the iron oxide structures and the mutual effects of coexisting cations on substitution for lattice Fe.

1. Introduction

Iron hydroxides are ubiquitously occurred in environmental, geological, and planetary systems, and exist in a number of polymorphs with variable structure order and crystal size depending on the conditions they crystallized (Cornell and Schwertmann, 2003; Navrotsky et al., 2008). Goethite, α-FeOOH, is the most widespread iron oxyhydroxide in near-surface environment of the Earth, e.g. soils and lake sediments (Cornell and Schwertmann, 2003; Lower et al., 2001; Lu et al., 2019a; van der Zee et al., 2003), owing to its high

* Corresponding author.
E-mail address: liufan@mail.hzau.edu.cn (F. Liu).

https://doi.org/10.1016/j.chemgeo.2019.119378
Received 18 August 2019; Received in revised form 2 November 2019; Accepted 7 November 2019
Available online 09 November 2019
0009-2541/

thermodynamic stability (Cornell and Schwertmann, 2003; Guo and Barnard, 2013). Especially it is one of the most important active minerals in red soils, laterite, and lateritic bauxite deposits in tropical, subtropical, and temperate regions (Liu et al., 1994; Yin et al., 2016; Yu et al., 2016). Owing to its common nanophase, high specific surfaces, and enrichment of surface active sites and defects, goethite plays a critical role in controlling the biogeochemical cyclings of various environmentally relevant substances, such as C, N, P, and S and toxic heavy metals (Borch et al., 2010; Chen et al., 2015; Cornell and Schwertmann, 2003; Flynn and Catalano, 2018; Liu et al., 2019a; Yu et al., 2016).

During weathering, crystallization, and dynamic transformation of iron hydroxides in the natural environment, Fe^{2+} and/or Fe^{3+} is always crystallized with the presence of various exotic metal cations, and consequently, natural iron hydroxides are rarely pure (Cornell and Schwertmann, 2003; Singh and Gilkes, 1992). Iron hydroxide minerals accumulate these exotic metal cations mainly through adsorption, isomorphous substitution, and precipitation (Gerth, 1990; Huynh et al., 2003; Kaur et al., 2009a; Kaur et al., 2009b; Kaur et al., 2010; Swedlund et al., 2009). Isomorphous substitution of exotic cations into the mineral structures would affect the mineral physicochemical properties, and thus their environmental behaviors (Cornell and Schwertmann, 2003; Kaur et al., 2009a; Singh and Gilkes, 1992; Singh et al., 2010).

Natural goethite minerals in soils are usually found to accommodate quite a large amount of various exotic metal cations (Cornell and Schwertmann, 2003; Dublet et al., 2017; Norrish and Taylor, 1961; Singh et al., 2010). Aluminum has the highest substituted level in goethite structure and can be as high as ~33 mol% (Schwertmann and Carlson, 1994). For other cations, the incorporation level into goethite structure is generally higher for trivalent ions (V^{3+}, Cr^{3+}, Mn^{3+}, Co^{3+}, Ga^{3+}) than divalent (Ni^{2+}, Cu^{2+}, Zn^{2+}, Cd^{2+}, Pb^{2+}) and tetravalent cations (Ti^{4+}, Th^{4+}) (Singh et al., 2010; Yin et al., 2018). Of the common trivalent cations that substitute Fe in goethite, Mn^{3+} and Co^{3+} are sensitive to redox conditions. Mn always exists in +3 after incorporation into goethite structure (Dublet et al., 2017; Liu et al., 2018; Wells et al., 2006), while Co can be either Co^{2+} or Co^{3+} in goethite lattice (Alvarez et al., 2008; Alvarez et al., 2015; Dublet et al., 2017; Pozas et al., 2004). It was reported that Co-substituted goethite synthesized by oxidation and precipitation of Fe^{2+} and Co^{2+} in sodium carbonate solution contained Co(II) in lattice (Pozas et al., 2004) while that synthesized by precipitation of Fe^{3+} and Co^{2+} in potassium hydroxide solution contained Co(III) in lattice (Alvarez et al., 2008; Alvarez et al., 2015; Pozas et al., 2004). In the uppermost lateritic horizons in a 64 m thick lateritic regolith developed upon peridotites in New Caledoni, Co occurred as Co(II) replacing for lattice Fe(III) in goethite (Dublet et al., 2017). At a Co content of 10 mol%, Co(II) substitution for Fe in goethite slightly increased the lattice parameters and cell volume (Pozas et al., 2004). Co(III) substitution for Fe in goethite gradually reduced the lattice parameters and cell volumes with the increase of Co content (Alvarez et al., 2008). However for a series of Co-substituted goethites samples with Co contents of 0–9.5 mol%, lattice parameter *b* gradually decreased with the Co content, but the cell volume firstly increased at a Co content of 0.5 mol% and then gradually decreased. Though X-ray diffraction and thermal analysis suggested the predominant presence of Co^{3+}, the exact Co oxidation state was not clear (Gasser et al., 1996).

Natural goethites usually contain more than one exotic cations (Gerth, 1990; Manceau et al., 2000; Singh and Gilkes, 1992; Trolard et al., 1995; Yin et al., 2016). A few studies have documented the co-substitution of di- and multi-cations into goethite structure. (Kaur et al., 2009a; Kaur et al., 2009b; Kaur et al., 2010) studied the incorporation of multi-metals involving Cr/Cd/Pb/Zn/Cu into goethite. It was found that a general sequence of maximal metal substitution was Cu > Zn > Cr ~ Cd > Pb, which was different from that of single metal substitution (Kaur et al., 2009a; Kaur et al., 2009b). In another study of Co + Mn co-substituted goethites, no synergetic or antagonistic effects were detected between Co and Mn (Alvarez et al., 2015). However, co-incorporation of Al^{3+} with other cations into the goethite structure is noteworthy focused by taking into consideration the following facts about Al^{3+}: 1) the most abundant metal element in Earth's crust, 2) ubiquitous in rocks and soils, 3) its almost coincident mobilization with Fe during weathering, and 4) the most enrichment substituent in iron hydroxides (Cornell and Schwertmann, 2003; Liu et al., 2019a; Norrish and Taylor, 1961; Schwertmann and Carlson, 1994). Yet limited studies were conducted on this. Co-incorporation of Mn and Al into goethite increased the unit cell volume and various Me–Me (Me = Fe, Mn and Al) distances. The dissolution rate of the minerals in 6 M HCl at 318 K increased with increasing Mn content. Al was homogeneously distributed in the goethite structure while Mn tended to accumulate in the outer layers. And Mn^{3+} was found to inhibit Al^{3+} substitution for Fe^{3+} (Alvarez et al., 2007). Later a series of Mn + Co and Al + Co co-substituted goethites were then synthesized by the same authors in alkaline media by aging several ferrihydrites. Co in the samples was suggested to be Co^{3+} as Co-substituted goethites had markedly reduced cell parameters compared to that of the pure sample. Incorporation of Al was found to be larger than that of Co while the incorporation of Mn was similar to that of Co (Alvarez et al., 2015). Based on the results of our previous study on heavy metal speciations in contaminated soils that Cd was mainly associated with crystalline goethite enriched with a high amount of Al substitution (Yin et al., 2016), simultaneous incorporation of Al + Cd into goethite was conducted in laboratory to investigate the association mechanisms of Cd with goethite (Yin et al., 2018). It was found that coexisting Al hardly affected the incorporation of Cd into the goethite structure, but the presence of Cd would greatly hinder the replacement of lattice Fe by Al. However, the underlying mechanisms were unclear.

In the present study, a series of single Co-, Al- and Al + Co co-substituted goethite samples were synthesized at room temperature. Several techniques, including powder X-ray diffraction (XRD) with Rietveld structure refinement, transmission electron microscopy (TEM), X-ray photoelectron spectroscopy (XPS) and X-ray absorption fine structure spectroscopy (XAFS) and wet chemistry analysis (acidic dissolution experiments) were combined, aiming to address the following questions: (1) The exact Co oxidation states in the Co-containing samples, (2) The effects of Co- and Co + Al co-substitution on the physicochemical properties of goethite, (3) Whether there are synergetic or antagonistic effects of coexisting Co or Al on the incorporation of Al or Co into the goethite structure, and (4) Try to elucidate the mechanisms of the preferable substitution for Fe by Co over Al when both coexist. These results can provide deep insights into the associated mechanisms of coexisting cations with iron hydroxide minerals and more accurately predict the fates of heavy metal pollutants in natural environments.

2. Materials and methods

2.1. Sample preparation

Single Co-, Al-, and Co + Al co-substituted samples were prepared by homogeneous coprecipitation (Cornell and Schwertmann, 2003; Huynh et al., 2003; Yin et al., 2018). Typically, certain amounts of Fe $(NO_3)_3{\cdot}9H_2O$, $Al(NO_3)_3{\cdot}9H_2O$ and $Co(NO_3)_2{\cdot}6H_2O$ (Table S1) were dissolved in 500 mL ultrapure water (18.2 MΩ·cm resistance). Then, 300 mL of 5 mol·L^{-1} KOH solution was added at a rate of 5 mL·min^{-1} under stirring, and the suspension pH was maintained > 13. The above suspension was diluted to 2 L, and then aged at room temperature for 12 d, during which the container lid was opened and the suspension was stirred for ~2 h every day for gas exchange (Kaur et al., 2009a; Yin et al., 2018). After aging, the supernatant was discarded, and the remaining slurry was treated with 200 mL of 0.2 mol·L^{-1} oxalic acid/ammonium oxalate solution (pH = 3.0) by shaking in dark at a speed of 80 r·min^{-1} at room temperature for 2 h, in order to remove amorphous materials. After washed by centrifugation, the obtained solids were

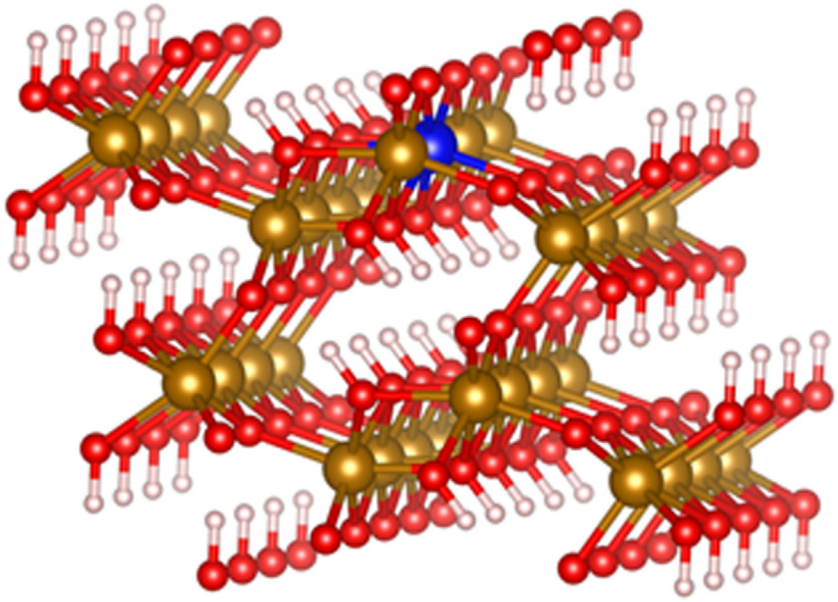

Fig. 1. The constructed supercell of goethite ($Fe_{31}MeO_{64}H_{32}$). Yellow balls represent Fe atom, red balls for O atom, blue balls for substituent Me (Al or Co atom), and white balls for H. (For interpretation of the references to colour in this figure legend, the reader is referred to the web version of this article.)

dried in an oven at 40 °C for several days and then ground and sieved through 100 mesh, and stored for further use. The obtained samples were named according to the nominal Co or Al concentrations. Single Co-substituted samples included GCoM (M = 1–9), single Al-substituted samples included 10AlG and 20AlG, and Co + Al co-substituted samples were named as NAlGCoM (*N* = 4, 10, 12 and 20; M = 1, 3 and 5).

2.2. Characterization

High resolution powder X-ray diffraction (XRD) patterns of the obtained samples were collected on a Bruker D8 ADVANCE diffractometer. The instrument was operated at a tube voltage of 40 kV and a current of 40 mA with Cu Kα radiation (λ = 0.15418 nm), and the scan rate was 1.2 s per step with a step size of 0.02° over a 2 theta range of 15–85°. Based on the goethite model (JCPDS 81-0464) and chemical compositions of the samples, Rietveld structure refinement was carried out using the TOPAS software (version 4.2) (Rietveld, 1969; Yin et al., 2018). Transmission Electron Microscopy (TEM) analysis was performed to observe the crystal morphology and particle size. The instrument (TEM, Philips-CM12) was operated at an acceleration voltage of 120 kV and an emission current of 10 μA. Samples were first dispersed in anhydrous ethanol by ultrasonication and then dropped on C-coated Cu grids. Cobalt 2p X-ray photoelectron spectra (XPS) were collected using a VG Multilab2000 X-ray photoelectron spectrometer with a Mg Kα X-ray source (1253.6 eV) using the large area mode with a pass energy of 25 eV and an energy step size of 0.1 eV. The non-charge corrected C 1s signal was set to 284.8 eV. Data were analyzed using Avantage software, and Shirley background was used (Yin et al., 2011).

The concentrations of Fe, Co, and Al in the obtained samples were determined by inductively coupled plasma atomic mass spectrometry (ICP-AES), after completely dissolving a small amount of sample powder (~0.1 g) in 10 mL of 6 M HCl solution in a 40 °C water bath. All analyses were done in triplicate.

2.3. X-ray absorption fine structure (XAFS) spectroscopy

The XAFS data of these samples were collected at beamline 1W1B at the Beijing Synchrotron Radiation Facility (BSRF) (Yin et al., 2012). Co K-edge data were collected in fluorescence mode over the energy range of 7509–8509 eV, and the energy correction (7709 eV) was performed with metal Co foil. Fe K-edge data were collected in transmission mode in the energy range of 6922–8012 eV, and the energy correction (7112 eV) was performed with metal Fe foil.

Data processing, including energy correction, background removal, and normalization were performed with IFEFFIT software (Ravel and Newville, 2005). The parameters used for background removal for Co were E0 = 7723 eV, Rbkg = 1, and k-weight = 2, while that for Fe K-edge spectra were E0 = 7126 eV, Rbkg = 1, and k-weight = 2. Fe K-edge EXAFS data were analyzed using several single scattering paths. Phase and amplitude functions for single-scattering paths were calculated using FEFF7 (Rehr et al., 1992), based on a goethite structure model (JCPDS 81-0464). Structural parameters (distance (R), coordination number (CN), and Debye-Waller factor (σ^2)) were obtained by fitting the experimental k^3-weighted EXAFS spectra to the standard EXAFS equation (Kelly et al., 2008) over a k range of 3.1 to 11.4 $Å^{-1}$ and an R range of 1–4 $Å^{-1}$. Hanning window function was used for the Fourier transform and EXAFS fitting.

2.4. Dissolution experiments

Dissolution behaviors of several samples were investigated with a single Co-substituted goethite (GCo3), a single Al-substituted sample (20AlG), and a Co + Al co-substituted goethite (20AlGCo3). Typically, 20 mg of the tested sample was dissolved in 400 mL of 2 mol·L^{-1} HCl solution at 25 °C under continuous constant stirring. About 5 mL of aliquot was withdrawn at predetermined time intervals, and then immediately filtered through a 0.22 μm membrane. Fe, Co, and Al concentrations in the filtrate were determined by ICP-AES.

2.5. Density function theory (DFT) calculations

The density functional theory (DFT) calculations were performed using the Vienna Ab-initio Simulation Package (VASP) to study the Al or Co substitution for Fe in goethite structure. The interaction between core electrons and valence electrons was described by the projector-augmented wave method (PAW). The Perdew – Burke-Ernzerhof (PBE) GGA-exchange-correlation functional was applied in calculations. The orbital-dependent corrections using DFT + U method with U = 4.0 was introduced for describing the localization of electrons on Fe3d levels (Belelli et al., 2014; Fuente et al., 2013; Zubieta et al., 2014). A large

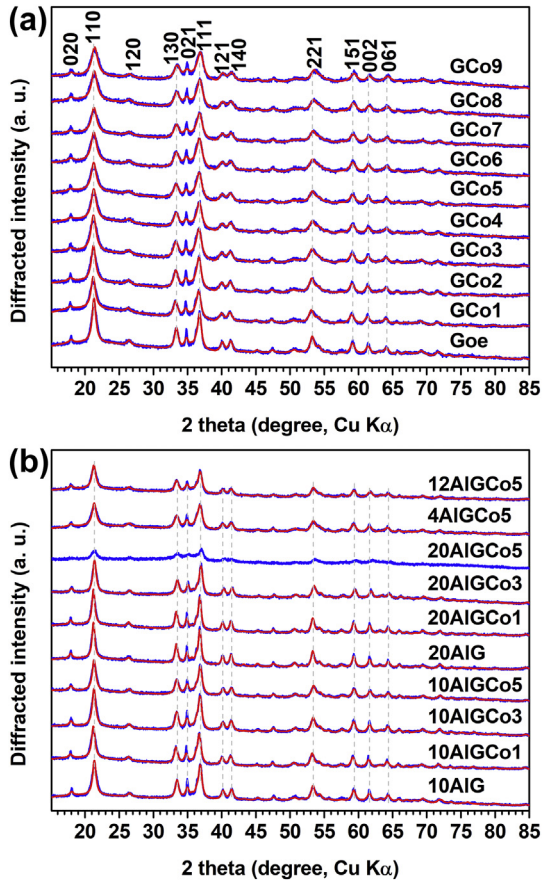

Fig. 2. Rietveld structure refinement of powder XRD patterns of singly Co-substituted (a) and singly Al-substituted and Co and Al co-substituted goethite samples (b). Blue lines are experimental data, and red lines are calculated patterns. (For interpretation of the references to colour in this figure legend, the reader is referred to the web version of this article.)

supercell size of ~128 atoms (1 × 3 × 2) was constructed for the calculation (Fig. 1). The calculated lattice parameters of bulk goethite were as follows: a = 10.0116 Å, b = 12.1175 Å, and c = 9.2431 Å, with an antiferromagnetic (AFM) arrangement, where each Fe atom was surrounded by other two Fe atoms with opposite magnetic-moments along the a-vector axis of the supercell (Belelli et al., 2014; Fuente et al., 2013; Zubieta et al., 2014). In relaxation, summations over the Brillouin zone (BZ) were performed using a 4 × 1 × 2 Monkhorst-Pack k-point mesh (Belelli et al., 2014). The smooth part of the wave functions was expanded in plane waves with a kinetic energy cutoff of 450 eV (Fuente et al., 2013). The convergence criteria for the ionic relaxation was $-0.02\ eV{\cdot}Å^{-1}$. The constructed pure supercell was labeled as Goe′, and the Al or Co substituted ones was labeled as AlG or GCo correspondingly.

3. Results and analysis

3.1. Powder XRD

Powder XRD patterns of these single Co-, Al-, and Co + Al co-substituted goethite samples are demonstrated in Fig. 2 and Fig. S1. They match well with that of goethite standard (JCPDS 81-0464). Incorporation of Co, Al, and Co + Al leads to the attenuation of peak intensities and increase of the full widths at half maxima (FWHMs) of the diffraction peaks. The peak positions also shift. With the increase of Co content, the (110), (130), (111), (221), (151), (002) and (061) peaks of single Co-substituted goethites gradually shift to the high angle. The peaks of Al-substituted goethites also shift to high angle with increasing Al dopant level. This suggests that Co or Al substitution for Fe in goethite lattice generally reduces unit cell parameters.

When the nominal Al concentration is 10 mol%, the peak intensities of goethite change little with the increase of Co dopant level from 0 to 5 mol% (Fig. 2b and Fig. S1b). When the nominal Al concentration is 20 mol%, the goethite peak intensities are greatly reduced with the increase of Co dopant level. And the peaks also shift to right slightly. When the nominal Co concentration is 5 mol%, the peak intensities are generally decreased with increasing Al concentration, and the peak positions also slightly shift toward right.

3.2. Chemical composition

The chemical compositions of the samples are listed in Table S2. Single Co-substituted goethites have final Co concentrations almost the same as the nominal ones. This implies that all Co is incorporated into the goethite structure. The maximum Co substitution level is 9.9 ± 0.3 mol%, which is close to that reported (Pozas et al., 2004). For Al-substituted goethites, when the nominal concentrations are 10 and 20 mol%, only 47–51% of the total Al are inserted into the goethite structure, and the maximum Al concentration is ~9.4 mol%. The reported maximum Al amount is ~33 mol% in synthetic or natural goethites (Schwertmann and Carlson, 1994). Many factors such as temperature, initial Al concentration, and use of Fe^{2+} or Fe^{3+} as precursor would affect the amount of Al substitution. Generally, goethite with high Al substitution for Fe could be formed at high pH and high initial Al^{3+} concentration, relatively low temperature and use of Fe^{2+} (Cornell and Schwertmann, 2003; Lewis, 1979a, 1979b; Lewis and Schwertmann, 1980). The use of Fe^{3+} as precursor may be the main reason that only half of the initial Al^{3+} is incorporated into the goethite structure.

When the initial concentrations of Al are constant, almost all the Co is inserted into the goethite structure with the increase of Co content, while the proportion of Al substitution is gradually decreased. In samples 10AlGCoM and 20AlGCoM (M = 1, 3 and 5), the contents of Co in the samples are 0.95–1.20, 3.15–3.32, and 5.38–6.07 mol%, respectively, when the initial Co concentrations are 1, 3, and 5 mol%. However, the final Al concentrations in 20AlGCoM samples (9.06–9.14 mol%) are higher than that in 10AlGCoM samples (6.46–7.13 mol%), especially when M = 1 and 3. When the initial Co contents are constant, the incorporation of Al into the goethite structure is reduced at high Co dopant level. At Co nominal concentration of 5 mol%, the final Co contents in NAlGCo5 (N = 4, 10, 12 and 20) are 5.18 ± 0.10, 5.38 ± 0.05, 5.10 ± 0.09, and 6.07 ± 0.03 mol% while the final Al contents are 3.13 ± 0.03, 5.74 ± 0.05, 8.11 ± 1.38, and 6.10 ± 0.01 mol%, respectively. The maximum dopant level for total exotic cations is 13.21 ± 1.38 mol% in 12AlGCo5.

3.3. Rietveld structure refinement

Rietveld structure refinements of these samples are conducted based on a goethite model (JCPDS 81 − 0464), and the results are presented in Figs. 2–4, Tables S2 and S3 and Fig. S2–S5. For the single Co-substituted goethites, unit-cell parameters a, b and c are generally decreased with increasing doping level. All three parameters are significantly negatively correlated with final Co concentrations in the samples (Fig. 3a, b, and c), with a number of independent data points (n) of 10 at a significance level (α) of 0.01. Correspondingly, unit-cell volumes (V) of these goethite samples are greatly reduced (Fig. 3d). These results are consistent with previous studies (Alvarez et al., 2008; Pozas et al., 2004). The calculated coherent scattering domain (CSD) sizes are also generally decreased with the increase of Co content (Fig. S2). The calculated crystal densities (ρ) of these single Co-substituted goethite samples have a significant positive linear relationship with the dopant level (Fig. 3e; n = 10, α = 0.01). For the single Al-doped goethites, unit

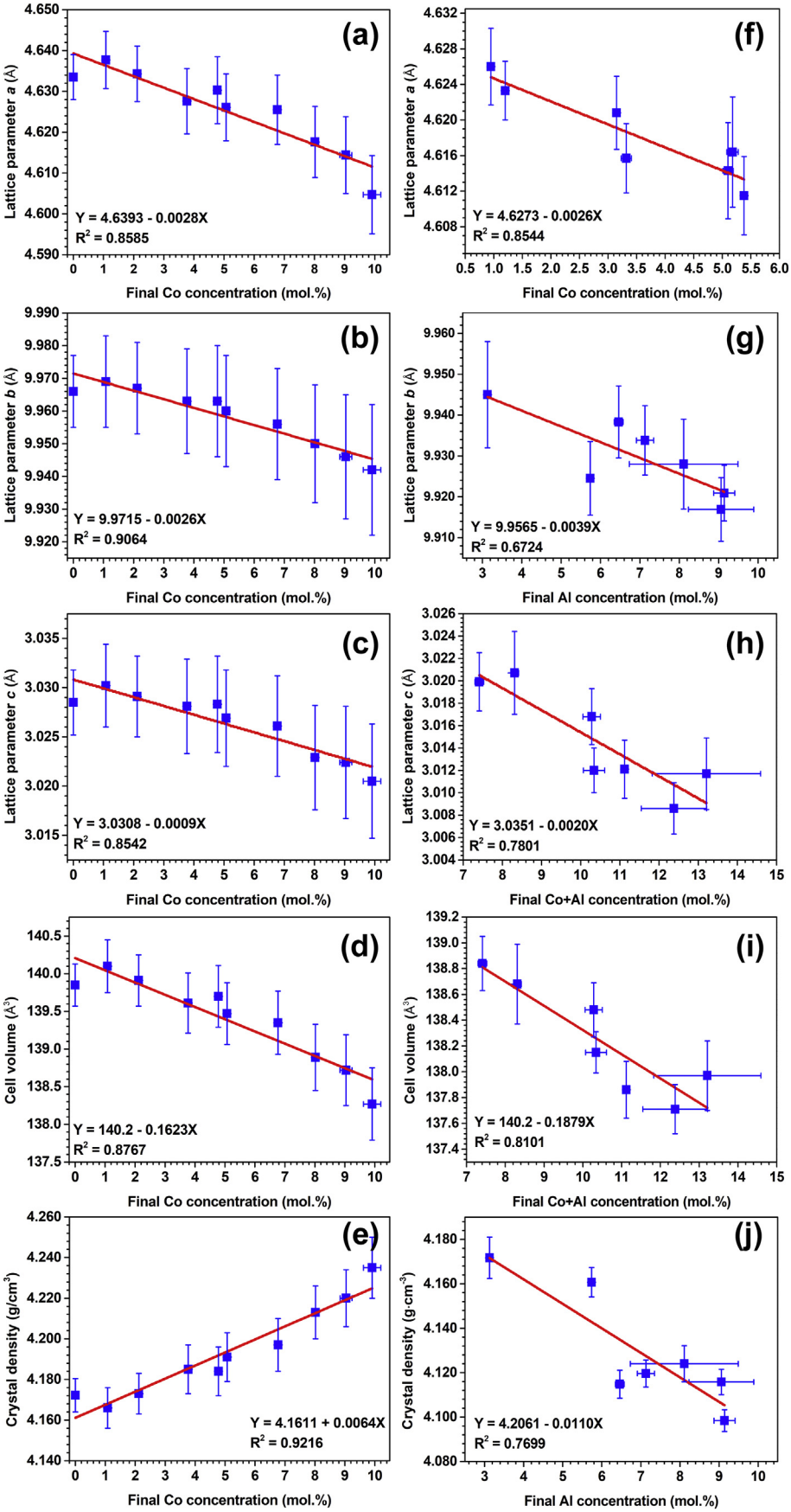

Fig. 3. Variations of lattice parameters (*a*, *b*, *c*), volume (V) and crystal density (ρ) of single Co-substituted goethites (a-e), and Co + Al co-substituted goethites (f-j) with the increase of final Co, Al, and Co + Al concentrations. Blue squares are experimental data, and red lines are the best linear fit. (For interpretation of the references to colour in this figure legend, the reader is referred to the web version of this article.)

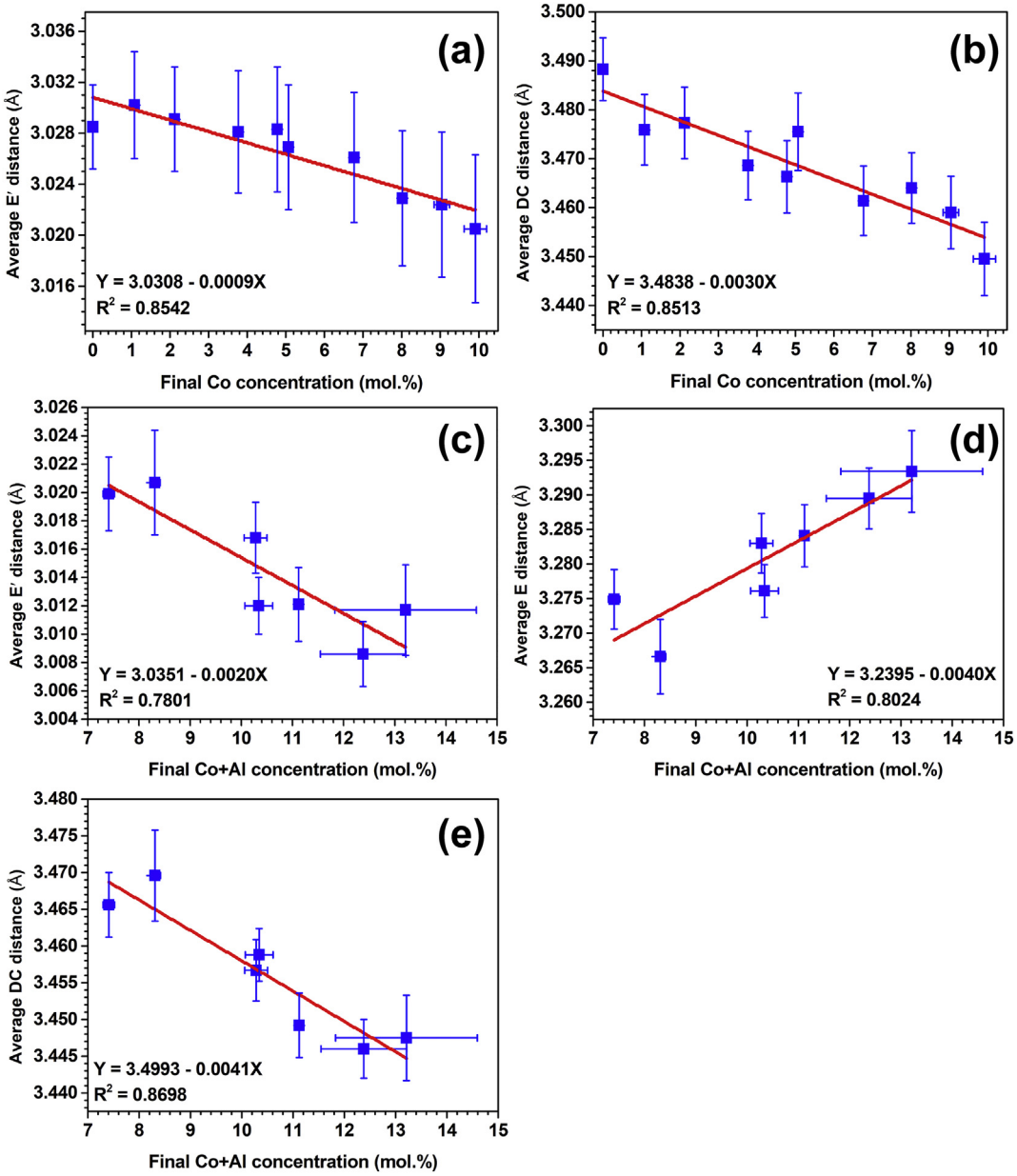

Fig. 4. Relationships of average edge-sharing Me−Me (Me = Fe, Al, and Co) distances along c axis (E') and along b axis (E), and average corner-sharing Me−Me (DC) distances with final Co and final Co + Al concentrations for single Co-substituted goethites (a-b) and for Co + Al co-substituted goethites (c-e).

cell parameters, V and ρ are gradually decreased while CSD sizes are increased with the increase of Al concentration (Table S2). But only lattice parameter *b* and ρ have significant negative linear relationships with the Al concentration in the samples at α levels of 0.05 and 0.10, respectively (Fig. S3).

For the Co + Al co-substituted goethites the relationships of the lattice parameters, V and ρ with the final Co, Al, and Co + Al contents are also analyzed, and the regression giving the largest R^2 is reported (Fig. 3f–j). It shows that various structure parameters depend on different factors. Lattice parameter *a* has the most significant negative linear relationship with the Co content in the sample (R^2 = 0.8544, n = 7, α = 0.05), lattice parameter *b* decreases linearly with the Al content (R^2 = 0.6724, n = 7, α = 0.10) while lattice parameter *c* has the best negative linear relationship with the total contents of Co + Al (R^2 = 0.7801, n = 7, α = 0.05). With the increase of total Al + Co content in the samples V values are linearly reduced (R^2 = 0.8101, n = 7, α = 0.05). The CSD sizes of these bi-substituted samples are gradually decreased with the increase of Co content (Fig. S4). The calculated ρ has a negative linear relationship with the final Al content in the sample (R^2 = 0.7699, n = 7, α = 0.05).

Rietveld structure refinement can also obtain the average bond lengths in the goethite structure. Three groups of Fe-Me (Me = Fe, Co, and Al) distances, e.g. edge-sharing Fe-Me distances E' (along c^* axis) and E (along b^* axis) and corner-sharing Fe-Me distance (DC) exists in goethite structures, besides Me-O distances in the [MeO_6] octahedron unit. Because of the different sizes of the dopants, substitution of Co or Al for Fe in the goethite structure may lead to changes in these Me-O and Fe-Me distances. The obtained Me-O distances, E′, E and DC of these doped goethite samples are listed in Table S3. The average Me-O, E′, E, and DC distances of pure goethite, Goe, are 2.103 ± 0.049, 3.029 ± 0.003, 3.262 ± 0.059, and 3.488 ± 0.006 Å, respectively. These values are almost the same as those in our previous study (Yin et al., 2018). Al incorporation generally results in a decrease of the E′ and DC distances but an increase of E (Fig. S5). With the highest Al concentration of 9.4 mol% in sample 20AlG, the average Me-O distance decreases to 2.042 ± 0.031 Å, and E′, E, and DC are 3.012 ± 0.002 Å,

3.308 ± 0.005 Å, and 3.431 ± 0.005 Å, respectively. For single Co-substituted goethite, increasing Co concentration results in corresponding increases in Me-O distances to 2.12–2.13 Å and E to 3.28–3.30 Å and decreases of E' and DC to 3.02–3.03 and 3.45–3.48 Å respectively. And both E' and DC have significant negative linear correlations with the Co dopant level (Fig. 4a, b).

For Co + Al co-substituted goethites with initial 10 mol% Al, the average Me-O, E′, and DC distances decrease to 2.007 ± 0.034, 3.012 ± 0.003, and 3.449 ± 0.004 Å, respectively while E increases to 3.284 ± 0.005 Å, when the initial Co concentration increases to 5 mol%. When the initial Al concent increases to 20 mol%, the average Me-O, E', and DC distances decrease to 2.023 ± 0.028, 3.009 ± 0.002, and 3.446 ± 0.004 Å, respectively, while E increases to 3.290 ± 0.004 Å, when the initial Co concentration increases to 3 mol%. For the co-substituted samples with initial Co concentrations to be 1, 3, and 5 mol%, when the initial Al concentration increases from 0 to 20 mol%, Me-O and E distances are firstly decreased with nominal Al concentration not above 10 mol% and then increased while E′ and DC are gradually decreased. No obvious relationship between the average Me-O distances and the final Al, Co, or Al + Co amounts in these Al + Co co-substituted goethites is observed. E' is found to have a significant negative linear correlation with the final Co + Al concentration (Fig. 4c; $R^2 = 0.7801$, $n = 7$, $\alpha = 0.05$). E is observed to have a significantly positive correlation with Co + Al amount (Fig. 4d; $R^2 = 0.8024$, $n = 7$, $\alpha = 0.05$). DC is decreased in a significant linear relationship with the increase of the total Co + Al amount (Fig. 4e; $R^2 = 0.8698$, $n = 7$, $\alpha = 0.05$).

3.4. Morphology

Morphologies of pure goethite, Goe, and typical single Al-, or Co-substituted and Co + Al co-substituted samples are observed by TEM (Fig. 5). Goe has the typical needle crystals of goethite (Alvarez et al., 2007; Cornell and Schwertmann, 2003; Kaur et al., 2010; Yin et al., 2018), and these needle crystals have an average length of 700 ± 206 nm and average width of 84 ± 23 nm (Table S5). Introducing ~9.4 mol% Al into the goethite structure greatly reduces the particle sizes in both length and width. 20AlG has the average length and width of 117 ± 24 and 16 ± 4 nm, respectively (Table S5), which are 17 ± 6% and 19 ± 7% of those of Goe. This suggests that with increasing A1 substitution the particle size of goethite becomes smaller, which coincides well with previous studies (Schulze and Schwertmann, 1984; Xu et al., 2019). For the Co-substituted sample, the length and width of the needle crystals are also decreased. For example, the average length and width of GCo5 are 429 ± 177 and 32 ± 7 nm respectively (Table S5). These values are 61 ± 31% and 38 ± 13% of those of Goe. The typical Al and Co bi-substituted sample, 4AlGCo5 has an average length and width of 187 ± 43, and 24 ± 6 nm, respectively (Table S5). Compared to GCo5, additional incorporation of ~3.1 mol% Al leads to 56 ± 21% and 25 ± 25% reduction in crystal width and length, respectively. Pure goethite crystals have an aspect ratio (width: length) of 0.12 ± 0.05. Cobalt substituted goethite, GCo5, has a smaller aspect ratio of 0.07 ± 0.03 than that of Goe. These changes in goethite after Co doping are the same as those observed in a previous study (Alvarez et al., 2015). Al substitution for Fe slightly increases the aspect ratio of the needle crystals. 20AlG has an aspect ratio of 0.14 ± 0.04 and 4AlGCo5 has an aspect ratio of 0.13 ± 0.04 which is larger than that of GCo5. Conclusively, the coexistence of Co, Al or Co + Al with Fe^{3+} greatly reduces the final goethite particle size. This may be associated with the retardation effects of these exotic cations on the nucleation, crystallization and crystal growth of the initially formed ferrihydrite and subsequently transformation of ferrihydrite to goethite (Cornell and Schwertmann, 2003; Huynh et al., 2003; Lu et al., 2019b). The coexistence of ferrihydrite with goethite crystals in samples with high total amount of Co + Al (e.g. 20AlGCo5; *session 4.2*) further confirms the suppression of exotic cations on the transformation of ferrihydrite into goethite.

3.5. Co 2p XPS spectra

Narrow scans of Co 2p XPS spectra of typical single Co- and Co + Al co-substituted goethite samples are plotted in Fig. 6. The binding energies (BEs) of Co $2p_{3/2}$ for GCo2, GCo5, GCo9, 20AlGCo5 and 4AlGCo5 range from 780.1–780.6 eV while the BEs of Co $2p_{1/2}$ range from

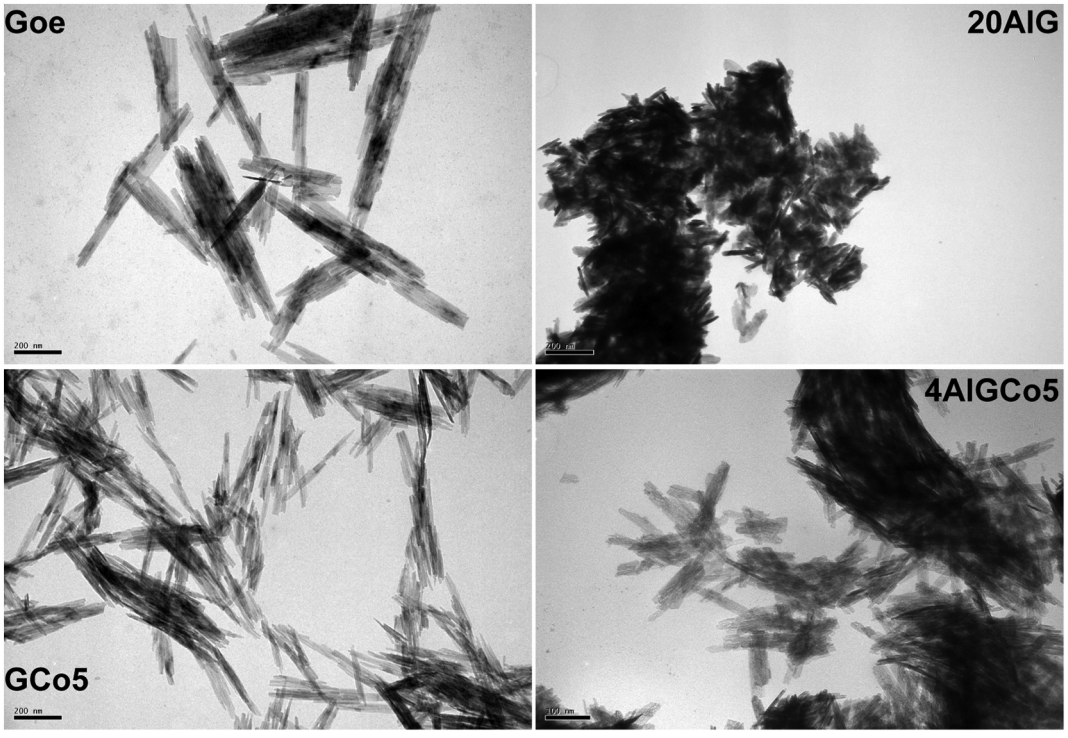

Fig. 5. TEM images of pure goethite, Goe, and typical single Al-, or Co-substituted, and Al + Co co-substituted samples.

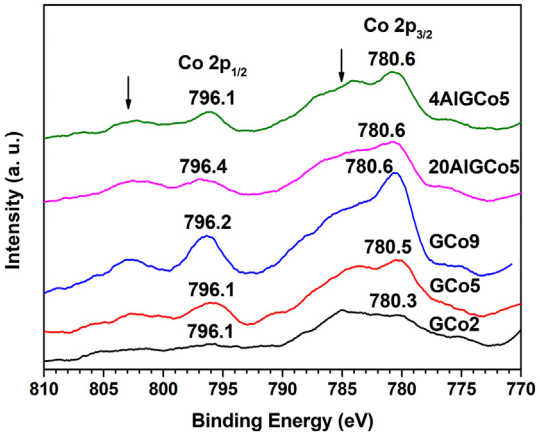

Fig. 6. Co 2p XPS spectra of typical Co-, and Co + Al co-doped goethite samples. Arrows indicate the satellite peaks arose from the presence of some Co^{2+} on the mineral surfaces.

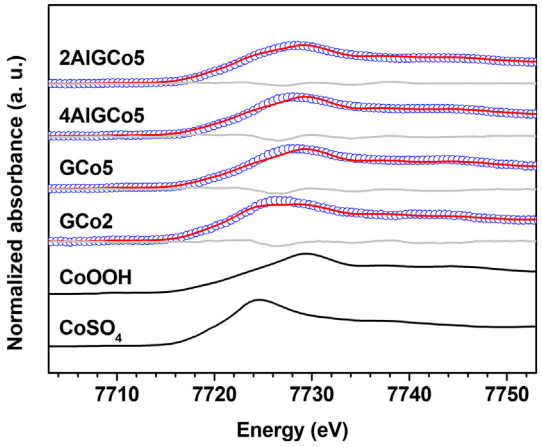

Fig. 7. Co K-edge XANES spectra of typical Co-, and Co + Al co-doped goethite samples, overlaid with the best linear combination fit using CoOOH and $CoSO_4$ as standards (Blue circles are experimental data, red lines are the best fit, and light gray lines are the difference patterns). (For interpretation of the references to colour in this figure legend, the reader is referred to the web version of this article.)

795.9–796.4 eV, respectively. These values are higher than those of CoOOH, but lower than those of $Co(OH)_2$ (Table 1) (Biesinger et al., 2011; Crowther et al., 1983). Further, the splittings of Co $2p_{3/2}$ and Co $2p_{1/2}$ (ΔBE) of these samples vary from 15.5 to 15.8 eV, which are larger than ΔBE for CoOOH (15 ± 0.1 eV) and closer to that for Co $(OH)_2$ (15.9 ± 0.1 eV) (Crowther et al., 1983). These results suggest that both Co(II) and Co(III) coexist in these samples, which can be also confirmed by the appearance of satellite peaks (indicated by arrows in Fig. 6) (Biesinger et al., 2011; Crowther et al., 1983). This is different from previous studies that Co existed as singly Co(II) (Pozas et al., 2004) or Co(III) in Co-substituted goethites (Alvarez et al., 2008; Alvarez et al., 2015; Gasser et al., 1996; Gerth, 1990; Pozas et al., 2002; Pozas et al., 2004). It was reported that when Co(II) was co-precipitated with Fe(II) at pH ~9, the Co existed in a valence of +2 while Co(III) incorporated into the goethite structure when Fe(III) and Co(II) solutions were co-precipitated at pH 12.5 (Pozas et al., 2004).

For single Co-substituted goethites, ΔBE decreases slightly from 15.8 eV for GCo2 to 15.6 eV for GCo9, which suggests more proportion of Co(II) in GCo2 than samples with higher Co content. At an initial Co content of 5 mol%, ΔBE slightly increases from 15.6 eV for GCo5 to 15.8 eV for 20AlGCo5. This may also suggest that Co + Al co-substituted samples with high Al contents may contain relatively higher proportions of Co(II) than samples contain no or low contents of Al.

3.6. X-ray absorption fine structure (XAFS) spectroscopy

3.6.1. Co K-edge XANES

Cobalt K-edge XANES spectra of typical Co-, and Co + Al co-doped goethite samples are presented in Fig. 7. As Co 2p XPS analysis indicates that Co in the samples exists as a mixture of Co(II) and Co(III), XANES spectra of reference materials CoOOH (Yin et al., 2013) and $CoSO_4{\cdot}7H_2O$ are used to analyze the relative proportions of various Co species in these goethites over an interval of 7703–7753 eV. The results are depicted in Fig. 6 and Table 1. It shows that GCo2 has 45 ± 2% Co^{2+} and 55 ± 2% Co^{3+} while GCo5 has 8 ± 2% Co^{2+} and 92 ± 2% Co^{3+}. That is, the proportion of Co^{3+} in single Co-substituted goethites greatly increases with increasing the Co content. For Co + Al co-substituted goethites the proportion of Co^{3+} decreases with the increase of Al incorporation. The proportion of Co^{3+} decreases from 90 ± 2% of 4AlGCo5 to 79 ± 1% of 20AlGCo5. These results are consistent with the results of Co 2p XPS analysis.

3.6.2. Fe K-edge EXAFS spectra

The Fe K-edge EXAFS spectra and corresponding Fourier transformed spectra (FTs) of typical single Al-, or Co-substituted, and Co + Al co-substituted goethite samples are illustrated in Fig. 8. These spectra are similar in amplitude, shape, and frequency, indicating that they essentially have similar local structure around Fe atoms. In the FTs there are mainly two peaks located at R + ΔR of ~1.5 and ~2.7 Å. The first peak corresponds to the Fe—O distance in [FeO_6] unit. The second peak, which is broad and has a shoulder at ~3.1 Å are convoluted by three Fe—Fe pairs, edge-sharing Fe-Me distances E' (along c^* axis) and E (along b^* axis) and corner-sharing Fe-Me distance (DC) existing in goethite structure (Manceau and Combes, 1988). Fitting of the Fe K-edge EXAFS spectra using several single scattering paths are conducted and the results are listed in Fig. 8 and Table 2.

It demonstrates that Goe has an average Fe—O distance, E′, E and DC of 2.003 ± 0.024, 3.011 ± 0.023, 3.220 ± 0.116, and 3.440 ± 0.036 Å, respectively. These values match well with those

Table 1
Binding energy values (BEs) for Co 2p XPS spectra and linear combination analysis results of Co K-edge XANES spectra of typical single Co- and Co + Al co-substituted goethites.

Sample	Co ($2p_{1/2}$) (eV)	Co ($2p_{3/2}$) (eV)	ΔBE[b] (eV)	Co(II)	Co(III)	R-factor	Reduced χ^2
GCo2	796.1	780.3	15.8	0.45(2)	0.55(2)	0.0084	0.0021
GCo5	796.1	780.5	15.6	0.08(2)	0.92(2)	0.0105	0.0029
GCo9	796.2	780.6	15.6	–	–	–	–
4AlGCo5	796.1	780.6	15.5	0.10(2)	0.90(2)	0.0078	0.0020
20AlGCo5	796.4	780.6	15.8	0.21(1)	0.79(1)	0.0050	0.0012
CoOOH[a]		780.20	15.1	–	–	–	–
$Co(OH)_2$[a]		781.00	15.9	–	–	–	–

[a] Data were from Crowther et al. (1983).
[b] ΔBE refers to the energy splittings of BEs of Co $2p_{1/2}$ and Co $2p_{3/2}$.

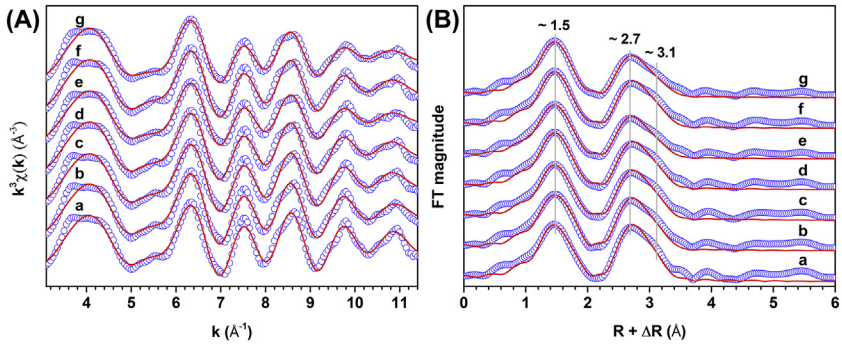

Fig. 8. Fe K-edge EXAFS spectra (A) and corresponding Fourier transformed (FTs) spectra (B) of single Co-, or Al-substituted, and Co + Al co-doped goethite samples (the blue circles are data and the red dash lines are the best fit). Goe, (b) GCo2, (c) GCo5, (d) 10AlG, (e) 20AlG, (f) 4AlGCo5, and (g) 20AlGCo1. (For interpretation of the references to colour in this figure legend, the reader is referred to the web version of this article.)

obtained by XRD Rietveld structure refinement. For single Al-substituted goethites, these Fe—O distance, E′, E, and DC are slightly decreased to 1.987 ± 0.024, 3.001 ± 0.025, 3.208 ± 0.112, and 3.394 ± 0.034 Å for 20AlG. For single Co-substituted goethites, these distances are 2.001 ± 0.027, 3.007 ± 0.025, 3.211 ± 0.097, and 3.399 ± 0.034 Å for GCo5. The obtained Fe—O, E′, E, and DC values for 20AlGCo1 are almost the same as those of 20AlG. These values are also the same for GCo5 and 4AlGCo5.

3.7. Dissolving behaviors

The dissolution curves for representative samples, GCo3, 20AlG, and 20AlGCo3, are displayed in Fig. 9. These samples undergo different dissolution behaviors. The release of Fe during the equilibrating of these minerals with 2 M HCl solution at 298 K is monitored (Fig. 9a). For the single Co-substituted sample, the release rate of Fe into solution is gradually increased before ~25 h, and then is gradually decreased till the end. After reaction for 132–156 h, the mineral is completely dissolved. The χ_{Fe}-t curve of the single Al-substituted goethite is much flatter than that of GCo3, indicating a much slower dissolution rate of 20AlG. After reaction for 432–504 h, all Fe in 20AlG is released into the solution. This suggests that Co promotes while Al retards the goethite dissolution. It is consistent with previous reports (Alvarez et al., 2008; Schwertmann, 1991). The difference in mineral dissolubility is ascribed to the much higher bond dissociation energy (BDE) of Al − O (502 ± 11 kJ·mol^{-1}) than that of Fe − O (407 ± 1 kJ·mol^{-1}) and the slightly lower BDE of Co—O (397 ± 9 kJ·mol^{-1}) than that of Fe—O (Lide and "Mickey" Haynes, 2010). However, the goethite dissolution in HCl solution is a much complex process, involving protonation, complexation, and reduction induced dissolutions by Cl^- (Cornell and Schwertmann, 2003). It can be affected by many other factors such as crystal sizes, coexisted cations, H^+ concentration and so on. Small particles are easier to be dissolved than big ones (Alvarez et al., 2007; Cornell and Schwertmann, 2003). Though 20AlGCo3 and 20AlG have almost the same contents of Al (~9.1 vs. ~9.4 mol%), additional insertion of ~3.3 mol% Co into the goethite structure greatly modifies the mineral dissolving behavior. The χ_{Fe}-t curve of 20AlGCo3 resembles more to that of GCo3 but with a slightly slower dissolution rate. The complete dissolution of 20AlGCo3 takes ~216 h. But during the first min, ~17% of total Fe is released into the solution. After reaction for 5 min, ~21% of total Fe is released, compared to ~1–2% in GCo3 and ~6% in 20AlG. This suggests that there is a small portion of poorly crystalline minerals, e.g. ferrihydrite, and/or small goethite particles in 20AlGCo3 (Liu et al., 2019b).

The corresponding Co or Al dissolving curves of these samples have similar shapes as the χ_{Fe}-t curves (Fig. 9b). Release of Co from GCo3 is much fast while the release of Al from 20AlG is much slower. The release curves of Co and Al from 20AlGCo3 are close to that of Co in GCo3. After reaction for 5 min, ~16% of total Co is released into the solution, which is much larger than that from GCo3 (~3%). These portions of Co in 20AlGCo3 may be associated with ferrihydrite and finite goethite particles.

The χ_{Fe}-t, χ_{Co}-t, and χ_{Al}-t curves are then fitted using the Kabai equation, $\chi_{Fe} = 1 - \exp(-(kt)^{\alpha})$, in which k is related to the dissolution rate and α is related to the characteristics of the mineral structure (Fig. 9a and b) (Kabai, 1973; Kaur et al., 2010). All curves are satisfactorily fitted except χ_{Fe}-t and χ_{Co}-t curves for 20AlGCo3, and the fitting results are depicted in Fig. 9a, b and Table 3. The obtained parameters are similar to previously reported values (Alvarez et al., 2007). Parameters α for GCo3 and 20AlG are similar, indicating the same basic structure of the matrix. But that for 20AlGCo3 is a bit smaller than that for GCo3 and 20AlG. This further confirms that the Fe atomic environments in 20AlGCo3 may be a little different from the other two. Parameters k for χ_{Fe}-t and χ_{Co}-t of GCo3 are almost the same, so are χ_{Fe}-t and χ_{Al}-t of 20AlG. But parameter k for χ_{Fe}-t of GCo3 is ~3.8 times that of χ_{Fe}-t of 20AlG. The Co dissolution rate from 20AlGCo3 is only a little smaller than that from GCo3.

The χ_{Co}-χ_{Fe} and χ_{Al}-χ_{Fe} curves of these samples are depicted in Fig. 9c, in company with a unit line through the origin. These χ_{Co}-χ_{Fe} and χ_{Al}-χ_{Fe} curves are almost overlapped with the unit line. This

Table 2
The structure parameters used to fit Fe K-edge EXAFS spectra of typical Al-, Co- and Co + Al co-substituted goethite samples.

Atomic pairs		Goe	10AlG	20AlG	GCo2	GCo5	20AlGCo1	4AlGCo5
Fe-O1	R (Å)	1.931(30)	1.932(31)	1.918(31)	1.927(32)	1.931(33)	1.924(29)	1.931(30)
	σ^2 (Å^2)	0.0038(23)	0.0042(25)	0.0049(24)	0.0041(25)	0.0045(26)	0.0047(24)	0.0041(24)
Fe-O1	R (Å)	2.075(38)	2.071(40)	2.055(36)	2.067(36)	2.071(42)	2.060(38)	2.073(41)
	σ^2 (Å^2)	0.0046(32)	0.0054(35)	0.0053(32)	0.0043(32)	0.0054(37)	0.0059(34)	0.0054(36)
E'	R (Å)	3.011(23)	3.011(24)	3.001(25)	3.007(23)	3.007(25)	3.003(25)	3.008(24)
	σ^2 (Å^2)	0.0038(26)	0.0051(30)	0.0062(32)	0.0037(24)	0.0045(29)	0.0062(30)	0.0047(27)
E	R (Å)	3.220(116)	3.225(108)	3.208(112)	3.217(82)	3.211(97)	3.206(114)	3.220(91)
	σ^2 (Å^2)	0.0139(244)	0.0131(209)	0.0151(232)	0.0092(114)	0.0116(167)	0.0157(224)	0.0107(142)
DC	R (Å)	3.400(36)	3.403(35)	3.394(34)	3.404(32)	3.399(34)	3.402(32)	3.404(34)
	σ^2 (Å^2)	0.0085(49)	0.0088(48)	0.0099(47)	0.0074(36)	0.0081(42)	0.0100(44)	0.0082(42)
E0(eV)		−5(4)	−5(4)	-6(4)	−5(4)	-5(4)	-5(4)	-5(4)
Chi Square		5963	6598	3626	6669	9269	6552	11,893
R-factor		0.0196	0.0200	0.0181	0.0199	0.0210	0.0172	0.0211

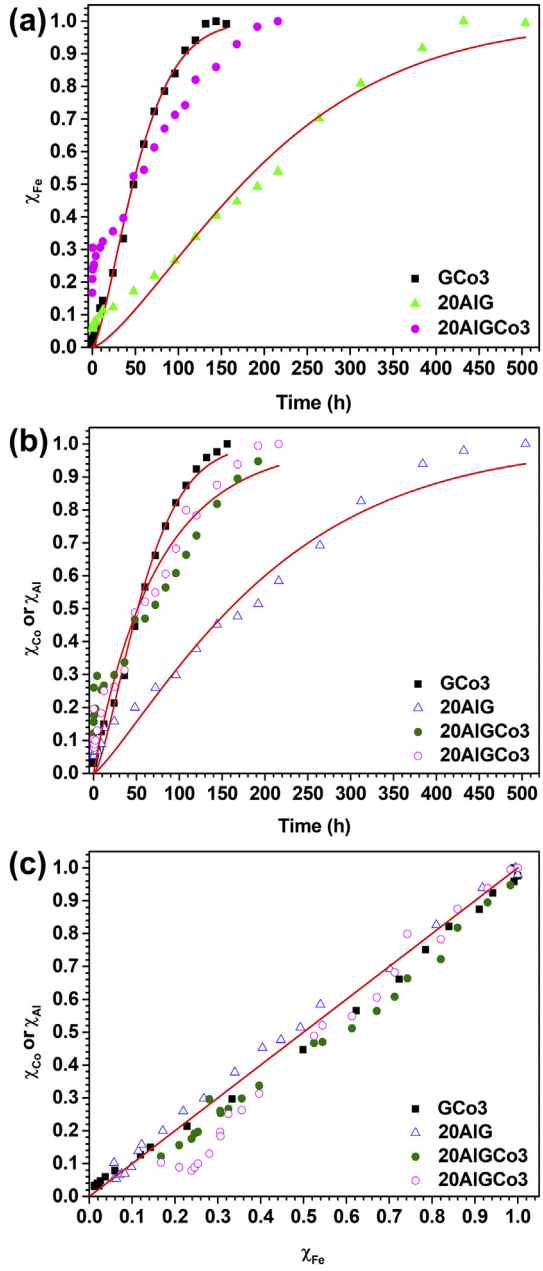

Fig. 9. Dissolution curves of typical samples in 2 M HCl solution at 298 K expressed as %Fe dissolved (χ_{Fe}) (a) and %Co or %Al dissolved (χ_{Co} or χ_{Al}) with time (b) and the corresponding χ_{Co}-χ_{Fe} or χ_{Al}-χ_{Fe} curves (c). Red solid curves in panels (a) and (b) are the best fit of the whole dissolution curve with Kabai equation, $\chi_{Fe(Co,\ Al)} = 1\text{-}\exp(-(kt)^{\alpha})$, in which k and α are constants representing the dissolution rate constant and the characteristics of the mineral structure (Kabai, 1973). In panels (b) and (c), solid symbols refer to Co while open symbols refer to Al. In panel (c), the red solid line is the 1:1 line. (For interpretation of the references to colour in this figure legend, the reader is referred to the web version of this article.)

suggests that Co or Al in these samples are probably evenly distributed in the goethite matrix by substitution for lattice Fe (Alvarez et al., 2006, 2007).

3.8. DFT calculations

In the constructed supercell, one Fe atom is replaced by an Al or Co atom, thus the Al or Co substitution level is 3.13 mol%. The lattice parameters (*a*, *b* and *c*) of Al-substituted goethite supercell (AlG) are calculated to be as follows: $a = 9.9860$ Å, $b = 12.1037$ Å, and $c = 9.2264$ Å while those for Co-substituted goethite supercell (GCo) are 9.9882 Å, $b = 12.0997$ Å, and $c = 9.2192$ Å correspondingly. These values are smaller than those of pure goethite supercell, indicating the contraction of cell dimensions after substitution of lattice Fe by Al or Co. This is also consistent with the results obtained by Rietveld structure refinement (Fig. 3, Fig. S3, and Table S2). The bond lengths (< 4 Å) of selected Fe—O and Fe-Me (Me = Fe, Al and Co) pairs of pure, Al- and Co-substituted goethite supercells obtained from DFT geometry optimization are listed in Table S4. The average Fe—O distances in [FeO_6] octahedra in supercells Goe′, GCo and AlG are 2.0395 ± 0.0795, 2.0384 ± 0.0764 and 2.0384 ± 0.0767 Å respectively. The average Fe-Me E′ distances are 3.0290, 3.0250 ± 0.0059 and 3.0260 ± 0.0062 Å for Goe′, GCo and AlG respectively, the corresponding E distances are 3.3255 ± 0.0011, 3.3250 ± 0.0141 and 3.3262 ± 0.0142 Å, and DC distances 3.4630 ± 0.0010, 3.4620 ± 0.0019 and 3.4623 ± 0.0027 Å respectively. These results agree well with those obtained by powder XRD Rietveld structure refinement and Fe K-edge EXAFS fitting.

The geometry optimized energy of constructed supercell $Fe_{32}O_{64}H_{32}$ in goethite is −797.646 eV. With one Fe atom in this supercell being replaced by one Al or Co atom, the supercell $Fe_{31}AlO_{64}H_{32}$ (AlG) or $Fe_{31}CoO_{64}H_{32}$ (GCo) was constructed, and the corresponding geometry optimized energy is −798.558 or −796.492 eV, respectively. Then the substitution energy ($\Delta E_{Me\ for\ Fe}$) is calculated according to the following equation:

$$\Delta E_{Me\ for\ Fe} = E(Fe_{31}MeO_{64}H_{32}) + E(Fe) - E(Fe_{32}O_{64}H_{32}) - E(Me) \quad (1)$$

in which Me refers to Al or Co atom in the present study.

The calculated $\Delta E_{Al\ for\ Fe}$ and $\Delta E_{Co\ for\ Fe}$ are −1.361 and 0.812 eV, suggesting that Al substitution for lattice Fe in goethite supercell is much more favorable than Co. However it should be noteworthy that all these calculations are conducted on Al or Co atoms, taking no consideration of cation size and charge.

4. Discussion

4.1. Oxidation state of Co in Co-containing goethites

Both Co 2p XPS analysis and linear combination analysis of Co K-edge XANES spectra show that Co exists as a mixture of Co^{2+} and Co^{3+} in these single Co- and Al + Co co-substituted goethite samples (Figs. 6, 7, and Table 1). For single Co-substituted goethites, the proportions of Co^{3+} in the mineral are gradually increased with the increase of the total amount of Co. For example, ~half of Co in GCo2 exists as Co^{2+} (Table 1). This coincides well with the changes of lattice parameters of single Co-substituted goethites with low Co contents (Fig. 3a–d and Table S2). The lattice parameters *a*, *b*, *c* and cell volume, V, of GCo1 and GCo2 are slightly larger than those of Goe. This is mainly caused by the relative larger coordination radius (CR) of Co(II) in octahedron (0.885 Å) than that of Co(III) (0.75 Å) and Fe(III) (0.785 Å) (Shannon, 1976). The increase of the proportion of smaller Co(III) substitution for Fe(III) linearly decreases the lattice parameters of single Co-substituted goethites. However, it was reported that Co existed as only Co(III) in single Co-substituted goethites (Alvarez et al., 2008; Pozas et al., 2004) and Co + Al and Mn + Co co-substituted goethites (Alvarez et al., 2015) synthesized using high concentration of NaOH solution or only Co(II) in single Co-substituted goethites synthesized using Na_2CO_3 solution (Pozas et al., 2004). The coexistence of Co(II) and Co(III) in our single Co-substituted goethites may be ascribed to the high pH but low aging temperature used during goethite synthesis. In these conditions, the precursor of goethite is ferrihydrite, which is a semiconductor mineral. Only when the electric potential energy in solution is higher than the conduction band energy of ferrihydrite, an electron can transfer to the ferrihydrite conduction band (CB) to oxidize Co^{2+} (Chernyshova, 2001a, 2001b, 2003; Chernyshova et al., 2011; Sander et al., 2015).

Table 3
Fitting parameters of the χ_{Fe}-t and χ_{Cd}-t curves of typical single Co-, Al-, and Co + Al co-substituted goethites in 2 M HCl solution at 25 °C using Kabai equation, χ_{Fe} or $\chi_{Cd} = 1\text{-}\exp(-(kt)^{\alpha})$ (Kabai, 1973).

	χ_{Fe}-t					χ_{Co}-t or χ_{Al}-t				
	k	error	α	error	R^2	k	error	α	error	R^2
GCo3	0.0165	0.0004	1.4337	0.0631	0.9953	0.0151	0.0004	1.4347	0.0854	0.9901
20AlG	0.0044	0.0004	1.3818	0.1287	0.9648	0.0047	0.0002	1.2144	0.1167	0.9617
20AlGCo3[a]	–	–	–	–	–	0.0132	0.0010	0.9516	0.1067	0.6451

[a] Kabai fitting of the χ_{Fe}-t and χ_{Co}-t curves for 20AlGCo3 are not successful.

However, the electric potential energy is related to the concentrations of redox cations (Boland et al., 2013), and only if the concentration of Co^{2+} is high enough that the electric potentional energy can drive electron transfer to the ferrihydrite CB to oxidize Co^{2+}. This is similar to the mechanisms involved in Mn^{2+} oxidation on iron oxides (Lan et al., 2017).

For Co + Al co-substituted goethites, the proportion of Co^{2+} is increased with the increment of the coexisting Al^{3+} content (Fig. 7 and Table 1). From Co5 to 20AlGCo5, the Co^{2+} proportion increases from 8 ± 2% to 21 ± 1%. This may be related to the specific properties of Al^{3+}. Owing to its small ionic radius (Shannon, 1976), Al^{3+} has much larger ionic potential (119.992 eV) than that of Co^{2+} (33.50 eV) and Fe^{3+} (54.8 eV) (Lide and "Mickey" Haynes, 2010). Consequently, Al^{3+} can retain OH^{-} more strongly than Co^{2+} and Fe^{3+}. This may cause a reduction in local alkalinity around Co^{2+}, which is unfavorable for Co^{2+} oxidation (Martí, 2002; Pozas et al., 2004).

4.2. Fe local environments in samples with high Co + Al substitution

Powder XRD patterns, Fe K-edge EXAFS analysis, and acid dissolution behaviors of all single Co- or Al-substituted goethites and Co + Al co-substituted samples with relatively low total contents of Co + Al confirm that they are pure goethite phase. However, Co + Al co-substituted samples with high total contents of Al + Co may contain a small amount of other poorly crystalline phases, such as ferrihydrite. Dissolution behaviors of 20AlGCo3, e.g. χ_{Fe}-t and χ_{Co}-t curves, differ from those of GCo3 and 20AlG, the χ_{Fe}-t and χ_{Co}-t or χ_{Al}-t curves of which can be fitted by Kabai equation successfully (Fig. 9). This may suggest that 20AlGCo3 may contain a small portion of ferrihydrite and/or small goethite particles (Liu et al., 2019b). It is thus expected that samples containing high total amounts of Co + Al synthesized in the present study may contain a portion of ferrihydrite. In the following, the Fe local environments in sample 20AlGCo5 are carefully investigated.

The powder XRD pattern of 20AlGCo5 is compared with that of 2-line ferrihydrite, 2LFh_1 (Wang et al., 2016) (Fig. 10A). There are two broad humps centered at ~35° and ~63° 2θ underneath the weak (130), (021) and (111) reflections, and (151) and (002) reflections of goethite, respectively. These two humps coincide well with the XRD pattern of 2LFh_1. This suggests that 20AlGCo5 is composed of goethite and 2-line ferrihydrite. This is further confirmed by Fe K-edge EXAFS analysis.

The Fe K-edge EXAFS spectra of single Al-, Co-, and Co + Al co-substituted goethites are compared with those of 2-line ferrihydrite, 2LFh_1 (Wang et al., 2016) (Fig. 10B and Fig. S6). The oscillations in the χ(k) of Goe has characteristics of pure goethite (Li et al., 2016; Waychunas et al., 2005). However, the spectrum of 2-line ferrihydrite has oscillations with greatly reduced magnitudes and is slightly left-shifted. Furthermore, the spectrum of the 2-line ferrihydrite can be distinguished from that of goethite by the two peaks located at ~5.2 $Å^{-1}$ and ~10.5 $Å^{-1}$ for ferrihydrite which are located at ~5.5 $Å^{-1}$ and ~10.9 $Å^{-1}$ for goethite (Fig. 10B and Fig. S6) (Li et al., 2016; Wang et al., 2016; Waychunas et al., 2005). The spectra of GCo2, GCo5, 10AlG, 20AlG, 4AlGCo5, and 20AlGCo1 are almost overlapped with that of Goe. In contrast, the spectrum of 20AlGCo5 resembles that of 2LFh_1 more than that of Goe (Fig. S6). This indicates that 20AlGCo5 contains a relatively large proportion of 2-line ferrihydrite.

In order to quantitatively analyze the proportion of 2-line ferrihydrite in these samples, linear combination fitting analysis (LCF) of Fe K-edge EXAFS spectra of these samples are conducted using Goe as pure goethite standard and 2LFh_1 as 2-line ferrihydrite standard. The fitting results are given in Fig. 10B and Table S6. It demonstrates that GCo2, GCo5, 10AlG, 20AlG, 4AlGCo5, and 20AlGCo1 have 10 ± 1%, 13 ± 1%, 16 ± 1%, 32 ± 1%, 18 ± 1% and 35 ± 1% 2-line ferrihydrite respectively. However, by taking consideration into the similarity of the Fe K-edge EXAFS spectra of these samples and the results of dissolution experiments, it is deduced that the error in 2-line ferrihydrite proportion determined by the LCF analysis here is ~35%. Thus, the proportion of 2-line ferrihydrite in 20AlGCo5 should be ~41%. This suggests that high total contents of Co and Al co-substitution would

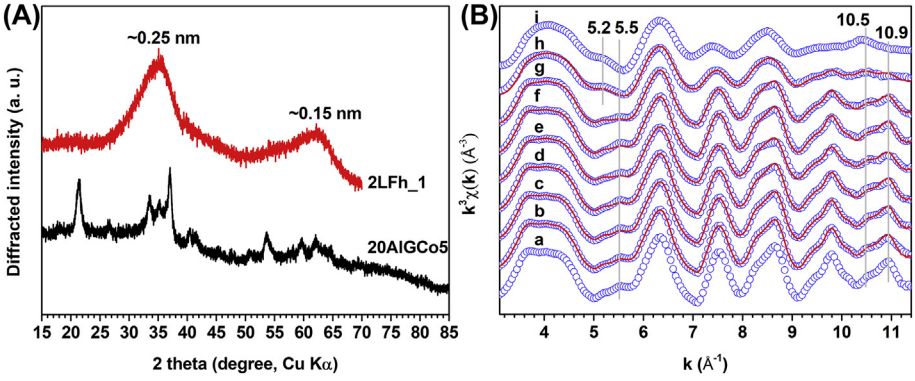

Fig. 10. (A) Powder XRD patterns of 20AlGCo5, in company with a pattern of 2-line ferrihydrite, 2LFh_1 from (Wang et al., 2016) to show that in the spectra of 20AlGCo5 the "humps" located at ~35° and ~63° probably correspond to the contribution from 2-line ferrihydrite phase. (B) Fe K-edge EXAFS spectra of these single Co-, Al-substituted and Co + Al co-substituted goethite samples, and a 2 line ferrihydrite sample, 2LFh_1 (Wang et al., 2016), overlapped with the best linear combination fittings of these Fe K-edge EXAFS spectra using Goe as goethite standard and 2LFh_1 as ferrihydrite standard (the blue circles are experimental data and the red lines are the best linear combination fittings).
(a) Goe, (b) GCo2, (c) GCo5, (d) 10AlG, (e) 20AlG, (f) 4AlGCo5, (g) 20AlGCo1, (h) 20AlGCo5 and (i) 2LFh_1. (For interpretation of the references to colour in this figure legend, the reader is referred to the web version of this article.)

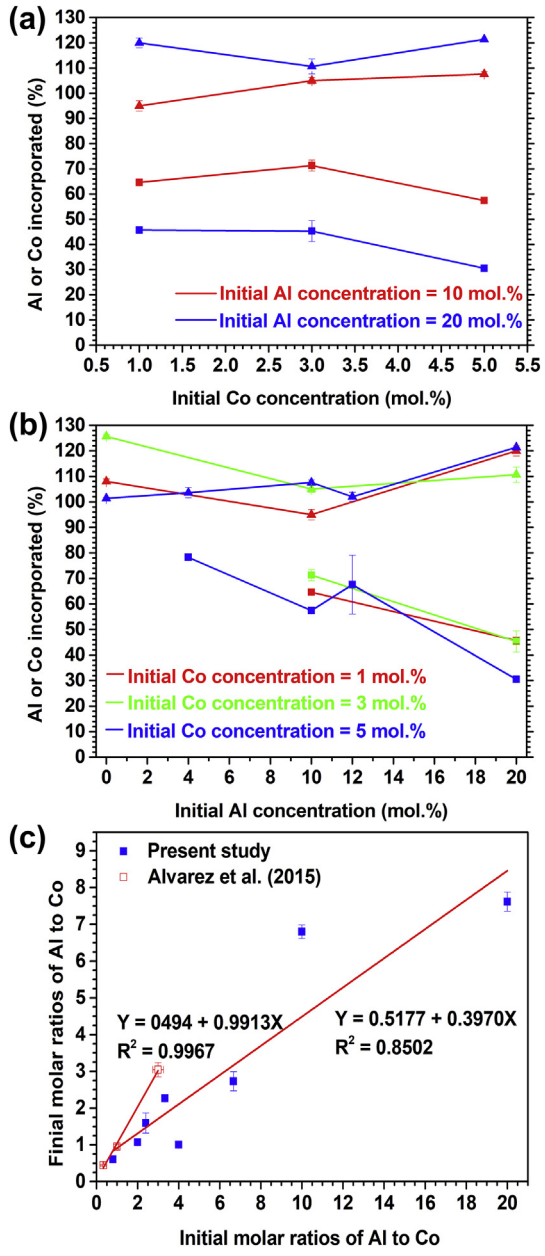

Fig. 11. The relationships of Co or Al incorporation ratio into Co + Al co-substituted goethites with (a) the increase of initial Co contents in 10AlGCoM and 20AlGCoM (M = 1, 3 and 5) and (b) the increase of initial Al contents in NAlGCo1, NAlGCo3 and NAlGCo5 (*N* = 0, 4, 10, 12 and 20) (■ for Al and ▲ for Co). (c) The relationship of final molar ratios of Al to Co in these Co + Al co-doped goethites (blue solid squares) with the initial molar ratios of Al to Co, and compared with those of Alvarez et al. (2015) (red blank squares). The red lines are the linear regression analysis of the data. (For interpretation of the references to colour in this figure legend, the reader is referred to the web version of this article.)

hinder the transformation of ferrihydrite into goethite.

4.3. Preference of Co over Al for substituting lattice Fe in goethite structure

Element analysis of Co and Al co-substituted goethites demonstrates that almost Co in the initial solutions are incorporated into the goethite structure while only a portion of the initial Al is inserted into the mineral. When the initial Al concentration is 10 mol%, 51 ± 1%, 65 ± 1%, 71 ± 2% and 57 ± 1% of the initial Al are incorporated into the mineral structure, while with the increase of Co from 0 to nominal 5 mol%. When initial Al concentration is 20 mol%, 47 ± 0%, 46 ± 1%, 45 ± 4%, and 31 ± 1% of the initial Al are retained in the mineral at the similar initial Co dopant level (Fig. 11a). At both Al dopant levels, the increase of coexisting Co content reduces the proportions of Al incorporated into the goethite structure. The incorporation of Al is further compared when the nominal Co content is kept constant at 1, 3, and 5 mol% (Fig. 11b). The proportion of Al incorporated decreases from 65 ± 1% in 10AlGCo1 to 46 ± 1% in 20AlGCo1 while that decreases from 71 ± 2% in 10AlGCo3 to 45 ± 4% in 20AlGCo3. At an initial Co concentration of 5 mol%, only 78 ± 1%, 57 ± 1%, 68 ± 12% and 31 ± 0.1% of the initial 4, 10, 12, and 20 mol% Al are incorporated into the minerals, respectively.

The final Al to Co molar ratios in these Co + Al co-substituted samples are plotted against the initial Al to Co molar ratios in the synthesis solutions, as shown in Fig. 11c. Linear regression analysis of these data gives a significant relationship ($R^2 = 0.8502$, $n = 8$, $\alpha = 0.01$) with a slope of only ~0.4. This value is almost the same as that observed in Cd + Al co-substituted goethites in our previous study (Yin et al., 2018). These results imply that the coexistence of Co suppresses the incorporation of Al into the goethite structure but Al has almost no effect on Co substitution for Fe. However, a previous study of Co and Al co-doped gothite samples did not detect any synergetic or antagonistic effects between Co and Al (Alvarez et al., 2015). The final Al to Co ratios and the initial Al to Co ratios in the previous study are also plotted in Fig. 9c. It also gives a good linear relationship ($R^2 = 0.9967$, $n = 3$, $\alpha = 0.10$) and a slope of ~1. The fact that predominance of Co over Al is observed in our study but not in the previous study may be related to the different synthesis protocols, especially the temperature and the concentration of OH^-, e.g. 25 °C and 0.75 mol·L^{-1} in present study in contrast to 60 °C and 0.3 mol·L^{-1} in the previous study (Alvarez et al., 2015).

The clear preference of Mn over Al or Cd over Al incorporation into the goethites was observed previously (Alvarez et al., 2007; Yin et al., 2018). It was concluded that coprecipitation reactions of cations with host minerals are affected by various physicochemical factors, such as pH, ionic strength, concentrations of substitution and host cations, cation complexation, temperature, and mineral precipitation rate (Curti, 1999; Wang and Xu, 2001). In the present study and our previous study (Yin et al., 2018), all these physicochemical factors are controlled and thus the focus is put on the properties of the dopant and host cations. The possible reasons for the Cd over Al incorporation into goethite structure were discussed in our previous paper in detail by symmetrically comparing the ionic radius, charge, bond dissociation energy (BDE), lattice energy, and the standard Gibbs free energy of formation (ΔG_f(aq)) (Yin et al., 2018).

As Co is next to Fe in the periodic table, many physicochemical properties of the two are similar. They have the same charge and the radius of high-spin (HS) state Co(III) (0.61 Å) is close to that of HS Fe (III) (Cornell and Schwertmann, 2003; Shannon, 1976). Both Co(III) and Fe(III) have almost the same BDE (397 ± 9 kJ·mol^{-1} vs 407 ± 1 KJ·mol^{-1}) (Lide and "Mickey" Haynes, 2010) and electronegativity ($\chi_{Co}^{3+} = 1.7614$, $\chi_{Fe}^{3+} = 1.7053$) (Portier et al., 1994; Shannon, 1976). All these similarities favor the incorporation of Co into the goethite structure. The BDE of Co—O is lower than that of Al—O (502 ± 11 kJ·mol^{-1}) implies a higher solubility of Co in ferrihydrite than Al in ferrihydrite and thus a larger incorporation rate of Co into goethite structure than Al. Co^{3+} is also more insoluble than Al^{3+} at high pH conditions, it is easier for $CoO_x(OH)_{6-x}$ unit to link with $FeO_x(OH)_{6-x}$ than for $AlO_x(OH)_{6-x}$ unit. However, our DFT calculations show a negative substitution energy of Al for Fe while a positive substitution energy of Co for Fe, implying the more favorable incorporation of Al atom into goethite supercell than Co atom. The obtained substitution energies, $\Delta E_{Al\ for\ Fe}$ and $\Delta E_{Co\ for\ Fe}$ are −131 and 78 kJ·mol^{-1} respectively. The substitution energy defined here is similar to the lattice energy difference (LED) (Dawson et al., 1985). For one mole atomic replacement, LED between Al and Fe was estimated to

be $-180\,kJ{\cdot}mol^{-1}$ while that between Co and Fe was $-55\,kJ{\cdot}mol^{-1}$ (Yin et al., 2018). Though both energies of Al substitution for Fe are similar, those for Co substitution for Fe differ much. This is probably ascribed to the consideration of charge and radius in the lattice energy calculation (Dawson et al., 1985). Thus both the physical (e.g. size and charge) and chemical (e.g. bonding ability, and chemical potential) properties of these cations should be considered.

A practical method to interpret the preference of one cation over the other was developed by (Wang and Xu, 2001) by correlating metal partition coefficients (K_d) with metal cation properties: $\Delta G_f(aq)$, the standard non-solvation energy ($\Delta G_n(aq)$), and the ionic radius, based on the linear free energy correlation established by (Sverjensky and Molling, 1992). The constants in this model can be determined by regression analysis of the data as long as K_d values of no less than three metals are available. Unfortunately, there is no such K_d value available for metal cations in goethite. Here thermodynamic partition coefficient is used as follows:

$$K_d = K_{sp}(\alpha\text{–FeOOH})/K_{sp}(\text{MeOOH}) \quad (2)$$

In which K_{sp}(α-FeOOH) and K_{sp}(MeOOH) are the thermodynamic solubility products of goethite and MeOOH (Curti, 1999). However not all the K_{sp} for M^{3+} are available, so only those for α-FeOOH, α-AlOOH, α-MnOOH, and CoOOH are used (Table 4), and then the corresponding thermodynamic K_d values of Al^{3+}, Mn^{3+}, or Co^{3+} incorporated in goethite structure are calculated and listed in Table 4.

Based on these thermodynamic K_d values, the linear free energy correlation model (Wang and Xu, 2001) was used to calculate K_d values of common trivalent cations in the goethite structure. The linear free energy relationship for crystalline solids and aqueous ions developed by Sverjensky and Molling (1992) correlates the standard Gibbs free energies of formation ($\Delta G_{f,MX}$) of minerals of an isostructural family (MX) with the ionic radius ($r_M{}^{Z+}$) and the standard non-solvation energy ($\Delta G_{n,M}{}^{Z+}$) of cation M^{Z+} as.

$$\Delta G_{f,MX} = a_{MX}{}^{*}\Delta G_{n,M}{}^{Z+} + \beta_{MX}{}^{*} r_M{}^{Z+} + b_{MX} \quad (3)$$

where $a_{MX}{}^{*}$, $\beta_{MX}{}^{*}$, and b_{MX} are characteristic constants of the isostructural family.

The ($\Delta G_{n,M}{}^{Z+}$) is the difference between the standard Gibbs free energy of formation ($\Delta G_{f,M}{}^{Z+}$) and solvation ($\Delta G_{s,M}{}^{Z+}$) of cation M^{Z+}:

$$\Delta G_{n,M}{}^{Z+} = \Delta G_{f,M}{}^{Z+} - \Delta G_{s,M}{}^{Z+} \quad (4)$$

in which $\Delta G_{s,M}{}^{Z+}$ is related to conventional Born solvation coefficient ($\omega_M{}^{Z+}$) (Shock and Helgeson, 1988).

$$\Delta G_{s,M}{}^{Z+} = \omega_M{}^{Z+}(1/\varepsilon - 1) \quad (5)$$

In this equation, ε is the dielectric constant (78.47) of water at 298 K, and $\omega_M{}^{Z+}$ is related to the charge (Z) and radius ($r_M{}^{Z+}$) of M^{Z+} (Sverjensky and Molling, 1992):

$$\omega_M{}^{Z+} = 166.027Z^2/(r_M{}^{Z+} + 0.94Z) - 53.87Z \quad (6)$$

According to Eqs. (3)–(6), $\omega_M{}^{Z+}$, $\Delta G_{s,M}{}^{Z+}$, and $\Delta G_{n,M}{}^{Z+}$ are calculated and listed in Table 4. Then these values are correlated to K_d values using.

$$\Delta G_{f,M}{}^{Z+} - 2.303RT\log K_d = a_{MHX}\Delta G_{n,M}{}^{Z+} + \beta_{MHX} r_M{}^{Z+} + b_{MHX} \quad (7)$$

The coefficients a_{MHX}, β_{MHX}, and b_{MHX} are constants and can be obtained by regression analysis. In the first step, the parameters of Fe^{3+}, Al^{3+}, Co^{3+}, Bi^{3+}, and Mn^{3+} were used for the regression analysis. However, the predicted (pred.) and experimental (exp.) k_d parameters for Mn^{3+} differ much. In further regression analysis, Mn^{3+} was ruled out. The regression gives $a_{MHX} = 0.78 \pm 0.03$, $\beta_{MHX} = 243 \pm 10\,kcal{\cdot}mol^{-1}{\cdot}Å^{-1}$ and $b_{MHX} = -365 \pm 9\,kcal{\cdot}mol^{-1}$ respectively ($R^2 = 0.9994$). The predicted K_d parameters are close to those of experiments, except that for Mn^{3+} (Table 4). This may be related to the accuracy of the measurement of the K_{sp} value.

According to the predicted K_d values, the K_d of Co^{3+} is positive while all the other trivalent cations have negative K_d values. This clearly indicates that Co would be incorporated into goethite structure over Al when they coexist. The K_d for Mn^{3+} is also larger than that of Al^{3+}, which can explain the observed dominant effect of Mn over Al during incorporation into goethite (Alvarez et al., 2007). However, it should be noted that for metal incorporation into goethite, the K_d should be zero. But the predicted K_d value for α-FeOOH is not zero. This may be ascribed to many factors, including the accuracy in the measurement of K_{sp}, and the determined K_d and so on. More work is needed to accurately measure K_d values for metal incorporation into the goethite structure in the future.

5. Conclusions and environmental implications

A series of single Co-, Al-, and Co + Al co-substituted goethite samples were synthesized at room temperature. All the obtained samples were almost pure goethite, except that with the highest total content of Co + Al. Both Al and Co incorporation reduced the goethite crystallinity and the particle length and width. In single Co-substituted samples, Co existed as a mixture of Co^{2+} and Co^{3+} and the proportion

Table 4
The ionic radius, maximum level (ML) of incorporation (Me × 100/(Me + Fe)) in single substituted goethites, conventional Born solvation coefficient ($\omega_M{}^{3+}$), the standard Gibbs free energy of formation ($\Delta G_{fM}{}^{3+}(aq)$), the standard Gibbs free energy of solvation ($\Delta G_{sM}{}^{3+}(aq)$) and the standard non-solvation energy ($\triangle G_{nM}{}^{3+}(aq)$), thermodynamic solubility products of MOOH (K_{sp}), and calculated (exp.) and predicted (pred.) partition coefficients (K_d) for several trivalent cations in goethite structure.

M	$r_M{}^{3+}$ (Å)[a]	ML (mol.%)[b]	$\omega_M{}^{3+}$ (kcal/mol)	$\triangle G_{sM}{}^{3+}(aq)$ (kcal/mol)	$\triangle G_{fM}{}^{3+}(aq)$ (kcal/mol)	$\triangle G_{nM}{}^{3+}(aq)$ (kcal/mol)	$\log K_{sp}$[c]	$\log_{Kd}$	
								Exp.	Pred.
Fe	0.65	100	269.01	−265.58	−4.12	261.46	−42.97	0	−1.86
Al	0.535	33	283.77	−280.15	−115.87	164.29	−35.09	−7.88	−7.45
Ga	0.62	40	272.76	−269.29	−38.00	231.29	–	–	−4.01
La	1.14	–	215.72	−212.97	−164.00	48.97	–	–	−84.29
Ce	1.07	–	222.51	−219.68	−161.60	58.08	–	–	−75.29
Cr	0.62	12	272.76	−269.29	−51.50	217.79	–	–	−6.15
Co	0.61	12	274.03	−270.54	32.03	302.57	−50.00	7.03	8.15
Ti	0.76	–	255.78	−252.52	−83.60	168.92	–	–	−26.55
V	0.64	13	270.25	−266.81	−57.90	208.91	–	–	−9.30
Bi	0.96	–	233.69	−230.71	19.79	250.50	−9.40	−33.57	−33.28
Mn	0.645	15	269.63	−266.19	−20.30	245.89	−18.26	−24.71	−3.88

[a] Data are from Shannon (1976).
[b] Data are from Schwertmann and Carlson (1994), Kaur et al. (2009c), Martin et al. (1997), Pozas et al. (2004), Sileo et al. (2004), and Wells et al. (2006).
[c] Data for goethite (α-FeOOH), diaspore (α-AlOOH) and manganite (α-MnOOH) are adopted from Ball and Nordstrom (1991), data for BiOOH is adopted from Speight (2005) and that for CoOOH is adopted from Hem et al. (1985).

of Co^{3+} increased with increasing Co content. The lattice parameters (*a*, *b*, and *c*) and cell volume were gradually decreased while crystal density was increased as the Co contents increased. These parameters for single Al-substituted samples were gradually decreased with increasing Al content. For Co + Al co-doped goethites, Co also existed in a mixed-valence of +2 and +3, and the proportion of Co^{3+} decreased with increasing the coexisting Al^{3+} content. Lattice parameter *a* decreased with increasing Co content, lattice parameter *b* and crystal density decreased with increasing Al content, and lattice parameter *c*, cell volume, average Fe-Me (Me = Fe, Co and Al) distances E' and DC decreased with increasing total Co + Al contents while E decreased. Co and Al were uniformly distributed in goethite structure, and Co greatly promoted mineral dissolution in acidic conditions. Coexisting Al^{3+} had almost no effect on the incorporation of Co into goethite structure, but the presence of Co suppressed the substitution of Al for Fe. This can be rationally explained by the calculated partition coefficients (K_d) using the linear free energy relationship. The present work highlights the necessity to consider not only the substituent cation physical properties, e.g. size, charge, but also the chemical properties, including chemical bonding energy and chemical potential, and provides insights into the incorporation mechanisms of co-existing cations into the iron hydroxide minerals.

Though in the present study the goethite samples were synthesized at an extremely high pH, compared to those of most natural environment conditions, the observed preference of Co over Al here, Cd over Al in our previous study (Yin et al., 2018) and Mn over Al (Alvarez et al., 2007) might also exist in geological settings, based on the linear free energy correlation model. Natural iron hydroxide minerals commonly contain various impurities, the most common of which is Al^{3+}. After entering soils and sediments, quite a large part of heavy metals are associated with Fe minerals. Most previous studies about the retention mechanisms of metal pollutants on iron oxides used synthetic pure mineral to mimic natural minerals (Okazaki et al., 1986; Wang et al., 2019), however the existence of Al in iron oxide structure can greatly modify the association behaviors of metal pollutants with iron oxide minerals (Liang et al., 2019). All these results suggest that natural Al-substituted iron oxide minerals may have enhanced retention capacities for heavy metal pollutants, either by adsorption or coprecipitation. Thus, taking into full consideration the exact Al content in iron hydroxide minerals to evaluate and predict their roles in controlling the fate and mobility of heavy metals in environments is strongly suggested.

Declaration of interest statement

The authors declare that they have no known competing financial interests or personal relationships that could have appeared to influence the work reported in this paper.

Acknowledgments

We gratefully acknowledge Prof. Hailiang Dong and the two anonymous reviewers for their critical and very helpful comments on the manuscript. Prof. Huifang Xu at University of Wisconsin-Madison was greatly thanked for help on the interpretation of the linear free energy correlation model. Prof. Zimeng Wang from Fudan University and Dr. Weizhao from Northwest A&F University were greatly thanked for providing some thermodynamic data. Dr. Xiaoming Wang from Huazhong Agricultural University was acknowledged for providing the powder XRD pattern and XAFS data of a 2-line ferrihydrite sample. The authors gratefully thank the Natural Science Foundation of China (Nos. 41571448, 41771267) and the National Key Research and Development Program of China (No. 2016YFD0800403) for financial support. HY gratefully acknowledges funding from China Scholarship Council.

Appendix A. Supplementary data

Supplementary data to this article can be found online at https://doi.org/10.1016/j.chemgeo.2019.119378.

References

Alvarez, M., Rueda, E.H., Sileo, E.E., 2006. Structural characterization and chemical reactivity of synthetic Mn-goethites and hematites. Chem. Geol. 231 (4), 288–299.
Alvarez, M., Rueda, E.H., Sileo, E.E., 2007. Simultaneous incorporation of Mn and Al in the goethite structure. Geochim. Cosmochim. Acta 71 (4), 1009–1020.
Alvarez, M., Sileo, E.E., Rueda, E.H., 2008. Structure and reactivity of synthetic Co-substituted goethites. Am. Mineral. 93 (4), 584–590.
Alvarez, M., Tufo, A.E., Zenobi, C., Ramos, C.P., Sileo, E.E., 2015. Chemical, structural and hyperfine characterization of goethites with simultaneous incorporation of manganese, cobalt and aluminum ions. Chem. Geol. 414, 16–27.
Ball, J.W., Nordstrom, D.K., 1991. User's Manual for WATEQ4F, With Revised Thermodynamic Data Base and Text Cases for Calculating Speciation of Major, Trace, and Redox Elements in Natural Waters. pp. 91–183.
Belelli, P.G., Fuente, S.A., Castellani, N.J., 2014. Phosphate adsorption on goethite and Al-rich goethite. Comput. Mater. Sci. 85 (0), 59–66.
Biesinger, M.C., Payne, B.P., Grosvenor, A.P., Lau, L.W.M., Gerson, A.R., Smart, R.S.C., 2011. Resolving surface chemical states in XPS analysis of first row transition metals, oxides and hydroxides: Cr, Mn, Fe, Co and Ni. Appl. Surf. Sci. 257 (7), 2717–2730.
Boland, D.D., Collins, R.N., Glover, C.J., David Waite, T., 2013. An in situ quick-EXAFS and redox potential study of the Fe(II)-catalysed transformation of ferrihydrite. Colloids Surf. Physicochem. Eng. Aspects 435, 2–8.
Borch, T., Kretzschmar, R., Kappler, A., Cappellen, P.V., Ginder-Vogel, M., Voegelin, A., Campbell, K., 2010. Biogeochemical redox processes and their impact on contaminant dynamics. Environ. Sci. Technol. 44 (1), 15–23.
Chen, C., Kukkadapu, R., Sparks, D.L., 2015. Influence of coprecipitated organic matter on $Fe^{2+}_{(aq)}$-catalyzed transformation of ferrihydrite: implications for carbon dynamics. Environ. Sci. Technol. 49 (18), 10927–10936.
Chernyshova, I.V., 2001a. Anodic oxidation of galena (PbS) studied FTIR-spectroelectrochemically. J. Phys. Chem. B 105 (34), 8178–8184.
Chernyshova, I.V., 2001b. Anodic processes on a galena (PbS) electrode in the presence of n-butyl xanthate studied FTIR-spectroelectrochemically. J. Phys. Chem. B 105 (34), 8185–8191.
Chernyshova, I.V., 2003. An in situ FTIR study of galena and pyrite oxidation in aqueous solution. J. Electroanal. Chem. 558, 83–98.
Chernyshova, I.V., Ponnurangam, S., Somasundaran, P., 2011. Effect of nanosize on catalytic properties of ferric (hydr)oxides in water: mechanistic insights. J. Catal. 282 (1), 25–34.
Cornell, R.M., Schwertmann, U., 2003. The Iron Oxides: Structure, Properties, Reactions, Occurences and Uses. Wiley-VCH, Weinheim.
Crowther, D.L., Dillard, J.G., Murray, J.W., 1983. The mechanisms of Co(II) oxidation on synthetic birnessite. Geochim. Cosmochim. Acta 47 (8), 1399–1403.
Curti, E., 1999. Coprecipitation of radionuclides with calcite: estimation of partition coefficients based on a review of laboratory investigations and geochemical data. Appl. Geochem. 14 (4), 433–445.
Dawson, B.S.W., Fergusson, J.E., Campbell, A.S., Cutler, E.J.B., 1985. Distribution of elements in some Fe-Mn nodules and an iron-pan in some gley soils of New Zealand. Geoderma 35 (2), 127–143.
Dublet, G., Juillot, F., Brest, J., Noël, V., Fritsch, E., Proux, O., Olivi, L., Ploquin, F., Morin, G., 2017. Vertical changes of the Co and Mn speciation along a lateritic regolith developed on peridotites (New Caledonia). Geochim. Cosmochim. Acta 217, 1–15.
Flynn, E.D., Catalano, J.G., 2018. Influence of oxalate on Ni fate during Fe(II)-catalyzed recrystallization of hematite and goethite. Environ. Sci. Technol. 52 (12), 6920–6927.
Fuente, S.A., Belelli, P.G., Castellani, N.J., Avena, M., 2013. LDA plus U and GGA plus U studies of Al-rich and bulk goethite (alpha-FeOOH). Mater. Chem. Phys. 137 (3), 1012–1020.
Gasser, U.G., Jeanroy, E., Mustin, C., Barres, O., Nuesch, R., Berthelin, J., Herbillon, A.J., 1996. Properties of synthetic goethites with Co for Fe substitution. Clay Miner. 31 (4), 465–476.
Gerth, J., 1990. Unit-cell dimensions of pure and trace metal-associated goethites. Geochim. Cosmochim. Acta 54 (2), 363–371.
Guo, H., Barnard, A.S., 2013. Naturally occurring iron oxide nanoparticles: morphology, surface chemistry and environmental stability. J. Mater. Chem. A 1 (1), 27–42.
Hem, J.D., Roberson, C.E., Lind, C.J., 1985. Thermodynamic stability of CoOOH and its coprecipitation with manganese. Geochim. Cosmochim. Acta 49 (3), 801–810.
Huynh, T., Tong, A.R., Singh, B., Kennedy, B.J., 2003. Cd-substituted goethites - a structural investigation by synchrotron X-ray diffraction. Clay Clay Miner. 51 (4), 397–402.
Kabai, J., 1973. Determination of Specific Activation Energies of Metal Oxides and Metal Oxide Hydrates by Measurement of the Rate of Dissolution.
Kaur, N., Gräfe, M., Singh, B., Kennedy, B., 2009a. Simultaneous incorporation of Cr, Zn, Cd, and Pb in the goethite structure. Clay Clay Miner. 57 (2), 234–250.
Kaur, N., Singh, B., Kennedy, B.J., 2009b. Copper substitution alone and in the presence of chromium, zinc, cadmium and lead in goethite (alpha-FeOOH). Clay Miner. 44 (3), 293–310.
Kaur, N., Singh, B., Kennedy, B.J., Gräfe, M., 2009c. The preparation and characterization of vanadium-substituted goethite: the importance of temperature. Geochim. Cosmochim. Acta 73 (3), 582–593.

Kaur, N., Singh, B., Kennedy, B.J., 2010. Dissolution of Cr, Zn, Cd, and Pb single- and multi-metal-substituted goethite: relationship to structural, morphological, and dehydroxylation properties. Clay Clay Miner. 58 (3), 415–430.
Lan, S., Wang, X.M., Xiang, Q.J., Yin, H., Tan, W.F., Qiu, G.H., Liu, F., Zhang, J., Feng, X.H., 2017. Mechanisms of Mn(II) catalytic oxidation on ferrihydrite surfaces and the formation of manganese (oxyhydr)oxides. Geochim. Cosmochim. Acta 211, 79–96.
Lewis, D.G., 1979a. The influence of Al on iron oxides. Part III. Preparation of Al goethites in M Koh. Clay Miner. 14 (2), 115–126.
Lewis, D.G., 1979b. The influence of aluminum on the formation of iron oxides. IV. The influence of [Al], [OH], and temperature. Clay Clay Miner. 27 (3), 195–200.
Lewis, D.G., Schwertmann, U., 1980. The effect of [OH] on the goethite produced from ferrihydrite under alkaline conditions. J. Colloid Interf. Sci. 78 (2), 543–553.
Li, W., Wang, L., Liu, F., Liang, X., Feng, X., Tan, W., Zheng, L., Yin, H., 2016. Effects of Al^{3+} doping on the structure and properties of goethite and its adsorption behavior towards phosphate. J. Environ. Sci. 45, 18–27.
Liang, Y., Wang, M., Xiong, J., Hou, J., Wang, X., Tan, W., 2019. Al-substitution-induced defect sites enhance adsorption of Pb^{2+} on hematite. Environ. Sci-Nano 6 (5), 1323–1331.
Lide, D.R., "Mickey" Haynes, W.M., 2010. CRC Handbook of Chemistry and Physics. CRC Press, Florida.
Liu, C., Chen, M., Li, F., Tao, L., Lin, J., Gao, T., Tong, H., Liu, Y., Long, S., Wu, F., Xia, Y., 2019a. Stabilization of Cd^{2+}/Cr^{3+} during aqueous Fe(II)-induced recrystallization of Al-substituted goethite. Soil Sci. Soc. Am. J. 83 (2), 483–491.
Liu, F., Xu, F., Li, X., Wang, Y., Zeng, G., 1994. Types of crystalline iron oxides and phosphate adsorption in variable charge soils. Pedosphere 4 (1), 35–46.
Liu, H., Lu, X., Li, M., Zhang, L., Pan, C., Zhang, R., Li, J., Xiang, W., 2018. Structural incorporation of manganese into goethite and its enhancement of Pb(II) adsorption. Environ. Sci. Technol. 52 (8), 4719–4727.
Liu, L., Wang, X., Zhu, M., Ma, J., Zhang, J., Tan, W.-F., Feng, X., Yin, H., Liu, F., 2019b. The speciation of Cd in Cd-Fe co-precipitates: does Cd substitute for Fe in goethite structure? ACS Earth Space Chem 3 (10), 2225–2236.
Lower, S.K., Hochella, M.F., Beveridge, T.J., 2001. Bacterial recognition of mineral surfaces: nanoscale interactions between *Shewanella* and α-FeOOH. Science 292 (5520), 1360–1363.
Lu, A., Li, Y., Ding, H., Xu, X., Li, Y., Ren, G., Liang, J., Liu, Y., Hong, H., Chen, N., Chu, S., Liu, F., Li, Y., Wang, H., Ding, C., Wang, C., Lai, Y., Liu, J., Dick, J., Liu, K., Hochella, M.F., 2019a. Photoelectric conversion on earth's surface via widespread Fe- and Mn-mineral coatings. P. Natl. Acad. Sci. 116 (20), 9741–9746.
Lu, Y., Hu, S., Wang, Z., Ding, Y., Lu, G., Lin, Z., Dang, Z., Shi, Z., 2019b. Ferrihydrite transformation under the impact of humic acid and Pb: kinetics, nanoscale mechanisms, and implications for C and Pb dynamics. Environ. Sci-Nano 6, 747–762.
Manceau, A., Combes, J.M., 1988. Structure of Mn and Fe oxides and oxyhydroxides: a topological approach by EXAFS. Phys. Chem. Miner. 15 (3), 283–295.
Manceau, A., Schlegel, M.L., Musso, M., Sole, V.A., Gauthier, C., Petit, P.E., Trolard, F., 2000. Crystal chemistry of trace elements in natural and synthetic goethite. Geochim. Cosmochim. Acta 64 (21), 3643–3661.
Martí, F.B., 2002. Química analítica cualitativa. Thomson.
Martin, F., Ildefonse, P., Hazemann, J.L., Mathe, P.E., Noack, Y., Grauby, O., Beziat, D., deParseval, P., 1997. Gallium crystal chemistry in synthetic goethites. J. Phys. IV 7, C2): 821–822.
Navrotsky, A., Mazeina, L., Majzlan, J., 2008. Size-driven structural and thermodynamic complexity in iron oxides. Science 319 (5870), 1635–1638.
Norrish, K., Taylor, R.M., 1961. The isomorphous replacement of iron by aluminum in soil goethites. J. Soil Sci. 12 (2), 294–306.
Okazaki, M., Takamidoh, K., Yamane, I., 1986. Adsorption of heavy metal cations on hydrated oxides and oxides of iron and aluminum with different crystallinities. Soil Sci. Plant Nutr. 32 (4), 523–533.
Portier, J., Campet, G., Etourneau, J., Tanguy, B., 1994. A simple model for the estimation of electronegativities of cations in different electronic states and coordinations. J. Alloy. Compd. 209 (1–2), 285–289.
Pozas, R., Ocaña, M., Morales, M.P., Serna, C.J., 2002. Uniform nanosized goethite particles obtained by aerial oxidation in the $FeSO_4$–Na_2CO_3 system. J. Colloid Interf. Sci. 254 (1), 87–94.
Pozas, R., Rojas, T.C., Ocana, M., Serna, C.J., 2004. The nature of Co in synthetic Co-substituted goethites. Clay Clay Miner. 52 (6), 760–766.
Ravel, B., Newville, M., 2005. Athena, Artemis, Hephaestus: data analysis for X-ray absorption spectroscopy using IFEFFIT. J. Synchrotron Radiat. 12 (4), 537–541.
Rehr, J.J., Zabinsky, S.I., Albers, R.C., 1992. High-order multiple scattering calculations of X-ray-absorption fine structure. Phys. Rev. Lett. 69 (23), 3397–3400.
Rietveld, H.M., 1969. A profile refinement method for nuclear and magnetic structures. J. Appl. Crystallogr. 2 (2), 65–71.
Sander, M., Hofstetter, T.B., Gorski, C.A., 2015. Electrochemical analyses of redox-active iron minerals: a review of nonmediated and mediated approaches. Environ. Sci. Technol. 49 (10), 5862–5878.
Schulze, D.G., Schwertmann, U., 1984. The influence of aluminium on iron oxides: X. Properties of Al-substituted goethites. Clay Miner. 19 (4), 521–539.
Schwertmann, U., 1991. Solubility and dissolution of iron oxides. Plant Soil 130 (1), 1–25.
Schwertmann, U., Carlson, L., 1994. Aluminum influence on iron oxides: XVII. Unit-cell parameters and aluminum substitution of natural goethites. Soil Sci. Soc. Am. J. 58 (1), 256–261.
Shannon, R., 1976. Revised effective ionic radii and systematic studies of interatomic distances in halides and chalcogenides. Acta Cryst 32 (5), 751–767.
Shock, E.L., Helgeson, H.C., 1988. Calculation of the thermodynamic and transport properties of aqueous species at high pressures and temperatures: correlation algorithms for ionic species and equation of state predictions to 5 kb and 1000 °C. Geochim. Cosmochim. Acta 52 (8), 2009–2036.
Sileo, E.E., Ramos, A.Y., Magaz, G.E., Blesa, M.A., 2004. Long-range vs. short-range ordering in synthetic Cr-substituted goethites. Geochim. Cosmochim. Acta 68 (14), 3053–3063.
Singh, B., Gilkes, R.J., 1992. Properties and distribution of iron oxides and their association with minor elements in the soils of south-western Australia. J. Soil Sci. 43 (1), 77–98.
Singh, B., Gräfe, M., Kaur, N., Liese, A., 2010. Chapter 8 - applications of synchrotron-based X-ray diffraction and X-ray absorption spectroscopy to the understanding of poorly crystalline and metal-substituted iron oxides. In: Balwant, S., Markus, G. (Eds.), Developments in Soil Science. Elsevier, pp. 199–254.
Speight, J.G., 2005. Lange's Handbook of Chemistry. MCGRAW-HILL, Wyoming.
Sverjensky, D.A., Molling, P.A., 1992. A linear free energy relationship for crystalline solids and aqueous ions. Nature 356, 231.
Swedlund, P.J., Webster, J.G., Miskelly, G.M., 2009. Goethite adsorption of Cu(II), Pb(II), Cd(II), and Zn(II) in the presence of sulfate: properties of the ternary complex. Geochim. Cosmochim. Acta 73 (6), 1548–1562.
Trolard, F., Bourrie, G., Jeanroy, E., Herbillon, A.J., Martin, H., 1995. Trace-metals in natural iron-oxides from Laterites - a study using selective kinetic extraction. Geochim. Cosmochim. Acta 59 (7), 1285–1297.
van der Zee, C., Roberts, D.R., Rancourt, D.G., Slomp, C.P., 2003. Nanogoethite is the dominant reactive oxyhydroxide phase in lake and marine sediments. Geology 31 (11), 993–996.
Wang, X., Zhu, M., Koopal, L.K., Li, W., Xu, W., Liu, F., Zhang, J., Liu, Q., Feng, X., Sparks, D.L., 2016. Effects of crystallite size on the structure and magnetism of ferrihydrite. Environ. Sci-Nano 3 (1), 190–202.
Wang, X.B., Chen, N., Zhang, L.Z., 2019. Enhanced Cr(vi) immobilization on goethite derived from an extremely acidic environment. Environ Sci-Nano 6 (7), 2185–2194.
Wang, Y., Xu, H., 2001. Prediction of trace metal partitioning between minerals and aqueous solutions: a linear free energy correlation approach. Geochim. Cosmochim. Acta 65 (10), 1529–1543.
Waychunas, G.A., Kim, C.S., Banfield, J.F., 2005. Nanoparticulate iron oxide minerals in soils and sediments: unique properties and contaminant scavenging mechanisms. J. Nanopart. Res. 7 (4), 409–433.
Wells, M.A., Fitzpatrick, R.W., Gilkes, R.J., 2006. Thermal and mineral properties of Al-, Cr-, Mn-, Ni- and Ti-substituted goethite. Clay Clay Miner. 54 (2), 176–194.
Xu, J., Koopal, L.K., Wang, M., Xiong, J., Hou, J., Li, Y., Tan, W., 2019. Phosphate speciation on Al-substituted goethite: ATR-FTIR/2D-COS and CD-MUSIC modeling. Environ. Sci-Nano. https://doi.org/10.1039/C9EN00539K.
Yin, H., Feng, X.H., Qiu, G.H., Tan, W.F., Liu, F., 2011. Characterization of Co-doped birnessites and application for removal of lead and arsenite. J. Hazard. Mater. 188 (1–3), 341–349.
Yin, H., Tan, W.F., Zheng, L.R., Cui, H.J., Qiu, G.H., Liu, F., Feng, X.H., 2012. Characterization of Ni-rich hexagonal birnessite and its geochemical effects on aqueous Pb^{2+}/Zn^{2+} and as(III). Geochim. Cosmochim. Acta 93, 47–62.
Yin, H., Liu, F., Feng, X.H., Hu, T.D., Zheng, L.R., Qiu, G.H., Koopal, L.K., Tan, W.F., 2013. Effects of Fe doping on the structures and properties of hexagonal birnessites - Comparison with Co and Ni doping. Geochim. Cosmochim. Acta 117, 1–15.
Yin, H., Tan, N., Liu, C., Wang, J., Liang, X., Qu, M., Feng, X., Qiu, G., Tan, W., Liu, F., 2016. The associations of heavy metals with crystalline iron oxides in the polluted soils around the mining areas in Guangdong Province, China. Chemosphere 161, 181–189.
Yin, H., Wang, Q., Li, Z., Li, W., Liu, L., Huang, C., Qiu, G., Feng, X., Tan, W., Xu, H., Liu, F., 2018. Effect of Cd and Al coincorporation on the structures and properties of goethite. ACS Earth Space Chem 2 (12), 1283–1293.
Yu, H.Y., Li, F.B., Liu, C.S., Huang, W., Liu, T.X., Yu, W.M., 2016. Chapter five - iron redox cycling coupled to transformation and immobilization of heavy metals: implications for paddy rice safety in the red soil of south China. In: Sparks, D.L. (Ed.), Advances in Agronomy. Academic Press, pp. 279–317.
Zubieta, C.E., Fortunato, L.F., Belelli, P.G., Ferullo, R.M., 2014. Theoretical study of SO_2 adsorption on goethite (110) surface. Appl. Surf. Sci. 314, 558–563.